HHS Public Access

Author manuscript

ACS Synth Biol. Author manuscript; available in PMC 2020 April 24.

Published in final edited form as:

ACS Synth Biol. 2019 April 19; 8(4): 744–757. doi:10.1021/acssynbio.8b00386.

A yeast system for discovering optogenetic inhibitors of eukaryotic translation initiation

Huixin Lu[1,†], **Mostafizur Mazumder**[1,†], **Anna S. I. Jaikaran**[1], **Anil Kumar**[1], **Eric Leis**[1], **Xiuling Xu**[1], **Michael Altmann**[2], **Alan Cochrane**[3], **G. Andrew Woolley**[1,*]

[1]Department of Chemistry, University of Toronto, 80 St. George St., Toronto, ON, M5S 3H6, Canada [2]Institut für Biochemie und Molekulare Medizin, Universität Bern, Bühlstr. 28; CH-3012 Bern, Switzerland [3]Department of Molecular Genetics, University of Toronto,1 King's College Circle, Toronto, ON M5S 1A8 Canada

Abstract

The precise spatiotemporal regulation of protein synthesis is essential for many complex biological processes such as memory formation, embryonic development and tumor formation. Current methods used to study protein synthesis offer only a limited degree of spatiotemporal control. Optogenetic methods, in contrast, offer the prospect of controlling protein synthesis non-invasively within minutes and with a spatial scale as small as a single synapse. Here, we present a hybrid yeast system where growth depends on the activity of human eukaryotic initiation factor 4E (eIF4E) that is suitable for screening optogenetic designs for the down-regulation of protein synthesis. We used this system to screen a diverse initial panel of 15 constructs designed to couple a light switchable domain (PYP, *Rs*LOV, LOV, Dronpa) to 4EBP2 (eukaryotic initiation factor 4E binding protein 2), a native inhibitor of translation initiation. We identified cLIPS1 (circularly permuted LOV inhibitor of protein synthesis 1), a fusion of a segment of 4EBP2 and a circularly permuted version of the LOV2 domain from *Avena sativa*, as a photo-activated inhibitor of translation. Adapting the screen for higher throughput, we tested small libraries of cLIPS1 variants and found cLIPS2, a construct with an improved degree of optical control. We show that these constructs can both inhibit translation in yeast harboring a human eIF4E *in vivo*, and bind human eIF4E *in vitro* in a light-dependent manner. This hybrid yeast system thus provides a convenient way for discovering optogenetic constructs that can regulate of human eIF4E-dependent translation initiation in a mechanistically defined manner.

Graphical Abstract

*To whom correspondence should be addressed: awoolley@chem.utoronto.ca, telephone: (416) 978-0675.
†These authors contributed equally

Supplementary Information: Detailed sequence data for all constructs, growth tests in yeast, Western blots, and controls for in-vitro translation and size-exclusion chromatography are available online at: acs_synthetic_biology

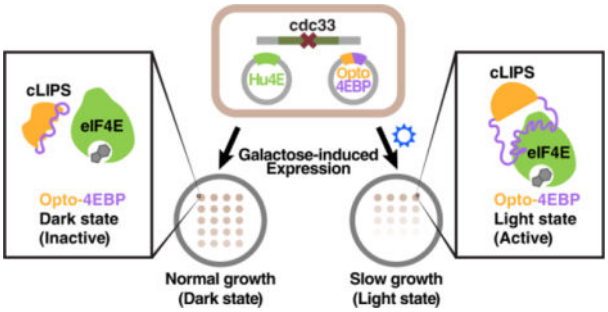

Keywords

photo-control; optogenetics; photoisomerization; genetically encoded; circular permutation; translation

The precise spatiotemporal control of protein synthesis (translation) is crucial for the function of cells and tissues in all organisms.[1, 2] At the level of a single cell, numerous points of control ensure appropriate translational responses, for example to changes in nutrient availability.[3, 4] In the brain, spatiotemporally-regulated translation plays a key role in the processes of learning and memory formation.[5, 6] Rapidly responsive translational machinery permits controlled expression of spatially localized pools of mRNAs in order to regulate synapse morphology and function.[7] Spatiotemporal control of translation is also vital for organismal development with translational responses occurring seconds to minutes after fertilization of the egg.[8]

Studying the roles of translation in these diverse settings requires tools that enable experimental control of translation. While, it is possible to manipulate translation by small molecule drugs or by expressing/injecting translational regulators, these approaches are limited when it comes to studying spatiotemporal changes in translation. Drugs cannot be spatially restricted with cellular or subcellular resolution, and cannot be quickly removed from cells. Tissue-specific promoters and viral vectors can permit spatial control of the expression of translational regulators, but temporal control is typically limited to hours or days,[9] whereas translation responses can occur in seconds to minutes.[10, 11]

Optogenetic approaches directly address the challenge of high-resolution spatiotemporal control.[12, 13] By using light to activate recombinant photoswitchable proteins that are expressed in specific tissues, spatiotemporal control of molecular function can be achieved within seconds and at subcellular resolution.[12, 13]

Several light-activated systems have been developed for the control of translation, including chemically modified “caged” RNAs that can be released using a light pulse,[14, 15] caged morpholinos or siRNAs that silence specific mRNAs,[16–18] or antagomirs that act on microRNAs.[19] Caged versions of the ribosome inhibitors, anisomycin,[20–22] emetine,[22] and puromycin,[23] and the mTORC1 inhibitor rapamycin,[21] have been reported as well as photo-regulated small molecule analogs of the 5’-mRNA cap.[24] These compounds allow precise timing but, with the exception of the cap analog, are irreversible. Moreover, they are not

genetically encoded so that they cannot be employed in a cell-type or cell-substructure-specific manner. Recently, Cao *et al.* have developed genetically-encoded optical controllers of translation using light-dependent interactions between CRY2 and CIB1 to co-localize the translation initiation factor eIF4E with mRNAs using specific RNA binding proteins.[25, 26] These are powerful tools for controlling cellular responses to specific mRNAs but cannot be used directly on native targets.[27] Moreover, this approach cannot produce the more global translational responses that naturally occur in response to a signaling event or growth.[11, 27]

Eukaryotic initiation factor 4E (eIF4E) is a key control point for the endogenous spatiotemporal regulation of translation. In the translation initiation step, eIF4E binds both the cap structure (m^7GpppN where N is any nucleotide) found at the 5' end of eukaryotic mRNA and eukaryotic initiation factor 4G (eIF4G), a large scaffolding protein[28, 29] The translation initiation machinery then assembles around eIF4G while eIF4E acts as a link between eIF4G and the mRNA (Figure 1A).[29] The interaction between eIF4E-eIF4G is tightly regulated by a family of eIF4E binding proteins (4EBPs)(Figure 1B). These proteins disrupt the eIF4E-eIF4G interaction by binding eIF4E and blocking eIF4G from interacting with eIF4E.[30]

In humans, three 4EBP homologues exist. For all homologues, the binding of 4EBP to eIF4E occurs through the consensus sequence YXXXXLϕ (X: any, ϕ: hydrophobic), termed the primary binding site, and is augmented by a more dynamic secondary binding site.[30, 31] The binding of 4EBP to eIF4E is regulated by phosphorylation of 4EBP at specific sites that lead to conformational changes and decreased affinity for eIF4E.[32] Peptides corresponding to segments of 4EBP containing the primary eIF4E binding site have been shown, using reporter assays, to inhibit translation in cell lysates[21, 33] and to inhibit translation-dependent processes when introduced *in vivo*.[34, 35] Since 4EBPs are well-characterized and highly conserved amongst higher eukaryotes, 4EBP-based designs (opto-4EBPs) would appear to be good candidates for optogenetic inhibitors of translation, suitable for probing spatiotemporal changes in translation in natural systems (Figure 1B).

It is important to stress that roles of 4EBPs in translational control are context dependent and, in a given cellular system, both global effects[36] or more focused effects on specific mRNA transcripts, and classes of mRNAs may be observed.[37, 38] Moreover, since translation is naturally subject to spatiotemporal control, exogenous manipulation of eIF4E via an opto-4EBP may activate compensatory homeostatic responses in a cell. For example, down-regulation of eIF4E expression using shRNA has been found to produce down-regulation, via ubiquitination and proteasomal degradation, of 4EBP.[39] Likewise, upregulation of eIF4E, often seen in cancer, can be accompanied by increases in hypophosphorylated forms of 4EBPs.[40] In addition to their central role in the initiation of translation, eIF4E and 4EBPs also function in nucleocytoplasmic transport of mRNA,[41, 42] sequestration of mRNA in a non-translatable state and stabilization of mRNA against decay in the cytosol.[43–45] An optogenetic inhibitor of translation must ultimately function by interfacing with this complex regulatory network, aspects of which are incompletely understood. Having tools with well-defined molecular activity, *i.e.* binding to eIF4E at the primary binding site, in a light-dependent manner, is thus an important first step towards a detailed understanding of this network.

To screen and characterize potential optogenetic inhibitors of translation acting in a defined manner through eIF4E, a suitable test platform is required. It is necessary to work with eukaryotes as bacteria use fundamentally different translation machinery. Additionally, to screen large numbers of potential constructs, a rapidly growing system, in which it is easy to introduce new genetic material, is ideal. For these reasons, we chose to use a modified yeast strain to develop a screening system. In both yeast and mammalian cells, eIF4E (encoded by CDC33 in yeast) is an essential gene and its disruption causes severe defects in growth.[46–48] Human eIF4E, and eIF4Es from numerous other species can functionally substitute for yeast eIF4E.[46–49] Native yeast eIF4E does not bind to mammalian 4EBPs.[50] We used a strain of *Saccharomyces cerevisiae* (Jo56) in which human eIF4E is expressed in a CDC33-deficient background. If human 4EBPs are expressed in this strain, translation is inhibited and growth is greatly slowed.[49–51]

Using this modified yeast strain, we expressed various 4EBP constructs designed to have photo-controllable activity (opto-4EBPs) and compared growth rates under light and dark conditions. Yeast expressing active opto-4EBPs were identified by slower growth in light compared to dark conditions. Using this assay, we identified a first-generation light-switchable opto-4EBP construct that we named cLIPS1 (**c**ircularly-permuted **L**OV **i**nhibitor of **P**rotein **S**ynthesis 1). Then, adapting the yeast assay for higher throughput screening, we were able to select improved mutants of the original construct, which we named cLIPS2. Using direct translation reporter assays, together with biochemical data on the purified proteins, we show that this yeast-based screening system enables discovery of constructs that impact translation initiation and can interact with human eIF4E in a light-dependent manner.

Results

Structure-based designs and screening

A panel of 15 candidate opto-4EBP constructs was created using insights gained from the design of current optogenetic tools and the structure of human 4EBP bound to eIF4E (Fig. 2, Fig. S1).[30, 52–54] Four different photoswitchable domains were fused to different lengths of human 4EBP2. Different lengths of 4EBP2 were used to vary the distance between the eIF4E binding sites and the photoswitchable domain. We used the 4EBP2 homolog because, although the 4EBPs appear functionally equivalent in terms of their primary and secondary binding sites for eIF4E, the 4EBP2 sequence exhibits the highest affinity for eIF4E.[31, 51, 55] Phosphorylation sites (S/T) of 4EBP2 were changed to Ala (for an alignment of sequences see Fig. S2) to avoid modulation of affinity for eIF4E by kinases.[32] The Lys57 residue that has been shown to be ubiquinated *in vivo* was not mutated since it is part of the primary binding site and effects of mutations of binding affinity have not been directly tested.[39] It is expected that the recognition of 4EBPs by the ubiquitination machinery will be different when segments are combined with photoswitchable proteins as is the case here. Finally, RAIP and TOS motifs that mediate mTORC1 and insulin-dependent phosphorylation of 4EBPs[56] are not included in these designs.

The four photoswitchable domains used were a LOV domain from *Rhodobacter sphaeroides* (RsLOV),[54] a LOV domain from *Avena sativa* (AsLOV2),[57] the green photoswitchable fluorescent protein Dronpa,[52] and photoactive yellow protein (PYP).[58] For the constructs

built with Dronpa and RsLOV, we reasoned that the dimerization of two Dronpa or RsLOV domains in the dark would sterically hinder ('cage') 4EBP2 and prevent 4EBP2 from binding to eIF4E.[52, 54] In the light, dissociation of the dimer would uncage 4EBP2 and allow binding to eIF4E.[52] Circular permutations of PYP and AsLOV2 were created so that the 4EBP2 sequence could be inserted between the original N- and C-terminal ends, which are the sites on these proteins that undergo the largest light-induced conformational changes.[58, 59] For the constructs built with cPYP, AsLOV2, and circularly permuted AsLOV2 we reasoned that the compact shape of the photoswitchable domain in the dark would sterically hinder 4EBP2 from binding to eIF4E.[60, 61] In the light, the additional flexibility of the proteins, would allow 4EBP2 to adopt its native conformation for binding to eIF4E.[57, 59, 62]

To screen these candidate opto-4EBPs for light-inducible inhibition of translation, we used Jo56, a strain of *S. cerevisiae* where CDC33 (the gene coding for yeast eIF4E) had been disrupted and human eIF4E is constitutively expressed from a plasmid[50] (Figure 3A). Plasmids containing galactose-inducible photoswitchable 4EBP2 constructs were transformed into this strain. Colonies were grown in synthetic media containing glucose (SC-W-U+Glu, see Methods), and then plated in serial dilutions onto two identical plates in which glucose was replaced by galactose (SC-W-U+Gal, see Methods) to induce expression of the opto-4EBP constructs. One plate was grown under ~450 nm blue light while the other was grown in the dark. A difference in growth between the light and dark plates was interpreted to mean that a construct impacted translation in its light-state versus its dark-state (Figure 3A, Fig. S3). Data from screens of all 15 constructs is shown in Figure S3. One construct, cLOV-V92I, showed very little growth inhibition in the dark but modest inhibition in the light (Figure 3B); we named this construct cLIPS1 (**c**ircularly-permuted **L**OV **i**nhibitor of **P**rotein **S**ynthesis 1).

Validating cLIPS1 activity (moved)

To confirm that cLIPS1 was inhibiting yeast growth through its effect on eIF4E, several control constructs were made. One negative control was made by mutating Leu51 and Leu52 in the primary binding site of cLIPS1 to Ala51, Ala52 (cLIPS1^{AA}). This mutation in full length 4EBP is known to abolish binding to eIF4E.[63] Another two negative controls were made by mutating Tyr46 to either Ala or Phe (cLIPS1^{Y46A} and cLIPS1^{Y46F} respectively). The Y46A mutation abolishes 4EBP binding to 4E while the Y46F mutation reduces binding to 5% of wild-type.[63] When cLIPS1^{AA}, cLIPS1^{Y46A}, and cLIPS1^{Y46F} were expressed in the Jo56 yeast strain, growth was comparable to wild-type (*i.e.* empty vector or AsLOV2) with no difference between light and dark (Figure 3B), indicating an intact eIF4E recognition site was necessary for cLIPS1 function.

When the 4EBP2 fragment found in cLIPS1 (tr-4EBP2) was expressed alone, yeast growth was strongly inhibited both in light and dark conditions (Figure 3B). Although there was some evidence of light toxicity at these low levels of growth, the effect was minimal compared to the inhibition of growth by cLIPS1 under blue light (Figure 3B). We note that several studies have reported detrimental effects of light on yeast growth due to production of reactive oxygen species.[64] We have also seen marked growth inhibition when high intensity blue light is used, and the effect is more pronounced with constructs that strongly

inhibit translation, such as with wild-type 4EBP2. Therefore, light levels for growth assays were carefully chosen to minimize these effects (see Methods section).

In past studies, it was found that human 4EBP1 and 4EBP2 did not affect the growth of yeast containing native yeast eIF4E, indicating the inhibition of growth observed in Jo56 in the presence of cLIPS1 is the result of an association between human 4E and the fragment of human 4EBP in cLIPS.[50, 51] As expected, when cLIPS1 and tr-4EBP2 were expressed in wild-type yeast, no inhibition of growth was seen in the light or the dark (Figure 3D).

The photoswitchable domain in cLIPS1 is a circularly permuted version of AsLOV2 (Figure 4A), the second light-oxygen-voltage domain of *Avena sativa* phototropin 1, containing a point mutation (V92I) known to slow the photocycle and thereby increase the light sensitivity.[65] AsLOV2 is an FMN-binding blue-light sensor, popular in many optogenetic designs.[66, 67] When AsLOV2 is irradiated with blue light, the FMN chromophore forms a bond with an adjacent cysteine, which causes the C-terminal Jα-helix and N-terminal A'α-helix of AsLOV2 to undock from the compact core of the protein.[59, 62] If the light source is removed, the flavin-cysteinyl bond breaks and AsLOV2 reverts to its dark state conformation.[59]

In cLIPS1, a fragment of human 4EBP2 connects the C-terminus of the Jα-helix to the N-terminus of the A'α helix. New N- and C-termini are inserted between the Hβ and Iβ strands creating a circular permutation of AsLOV2 (Figure 4A). The 4EBP2 fragment in cLIPS1 is comprised of the wild-type 4EBP2 sequence from position 51–85 with mutated phosphorylation sites (S65A and T70A). This length of 4EBP2 is the minimum needed to include both primary and secondary eIF4E binding sites, which are required for high-affinity binding to eIF4E.[30, 31, 68] We hypothesize that, in the dark, the N- and C- termini of native AsLOV2 hold the two binding sites of 4EBP2 in an unfavourable conformation for eIF4E binding. In the light, enhanced flexibility due to unfolding of the Jα-helix and A'α-helix then allows 4EBP2 to bind eIF4E (Figure 4B).

Library screening for increased light versus dark activity

To improve the difference in activity between light and dark states of cLIPS1, we took advantage of the yeast growth assay to enable higher-throughput screening. Two small libraries (one primer-based and the other error-prone) were made based on the cLIPS1 template. The primer-based library was aimed at varying the junctions between the 4EBP2 sequence and the cLOV sequence, whereas the error-prone library simply introduced mutations randomly between residue T16 and E104, which encompasses the 4EBP segment and parts of cLOV on either end (see Figure S1). These libraries were transformed into Jo56, grown in glucose, then replica plates were made on galactose media. One plate was grown in the light while the other was grown in the dark. From the primer-based library, we found one colony that showed a significant decrease in size when grown in the light compared to the dark (Figure 5A). This colony was picked and sequenced. Interestingly, the sequence showed a duplication of the secondary binding site on 4EBP2, an unexpected mutation that presumably arose from adventitious primer annealing to the starting sequences in the library. *In vivo* characterization in yeast showed that the construct, named cLIPS2, inhibited growth more strongly in the light compared to cLIPS1 (Figure 5B). A negative control of cLIPS2

with Leu51 and Leu52 mutated to alanines (cLIPS2^{AA}) also showed no impact on the growth of the yeast. We hypothesize that the duplication of the secondary binding site in cLIPS2 either enhances affinity for eIF4E by enhancing the local concentration of binding sites, and/or acts as a linker between the 4EBP2 and the cLOV sequence, increasing flexibility and accessibility in the light-state.

Growth curves and protein quantification in liquid culture

To confirm results obtained from yeast growth on plates, we also analyzed growth curves for Jo56 strains in liquid culture. Under low levels of blue light (50 μW/cm^2) in liquid culture, the growth of Jo56 expressing cLIPS1 and cLIPS2 showed significant differences between light and dark conditions (Figure 6A). The negative controls, AsLOV2, cLIPS1^{AA}, and cLIPS2^{AA}, all grew robustly with no difference between light and dark conditions, while the positive control, tr-4EBP2, grew poorly with no difference between light and dark. A doubling time was calculated for all six strains and no significant change was seen between light and dark doubling rates for controls (Figure 6B).[69]

Since a phenotypic screen may uncover switchable constructs that operate via a change in protein expression level or protein stability, rather than via allosteric effects on function,[70] we wished to test for possible light-dependent changes in cLIPS concentration. C-terminal myc-tags were therefore added to the AsLOV2, tr-4EBP2, wt-4EBP2, cLIPS1, cLIPS1^{AA}, cLIPS2, cLIPS2^{AA} constructs. We confirmed that the myc-tagged constructs behaved in the same manner as their un-tagged counterparts in yeast growth assays (Fig. S4), indicating that the tag did not interfere with construct activity. Yeast expressing myc-tagged constructs were then grown in liquid culture, under light and dark conditions, and expression levels of the constructs versus total protein or GAPDH (reported to be insensitive to eIF4E[71]) were determined by Western blot with an anti-myc antibody (Fig. S4). Constructs that had no effect on growth (AsLOV2, cLIPS1^{AA}, and cLIPS2^{AA}) expressed robustly with no difference between light and dark conditions. Interestingly, expression levels of the active constructs, cLIPS1 and cLIPS2, were ~2-fold lower than expression levels of negative controls under both light and dark conditions, with the expression of cLIPS2 under light conditions ~2.5 fold lower. These data show that the light-dependent inhibition of growth in yeast expressing cLIPS1 and cLIPS2 is not a result of higher expression of the constructs under light conditions, leading to increased metabolic burden or toxicity. We hypothesize that the observed *decreased* expression of active constructs could be due to a negative feedback effect, where cLIPS1 or cLIPS2 proteins inhibit their own expression (*vide infra*).

Polysome Analysis

To confirm that cLIPS constructs were inhibiting growth via inhibition of translation initiation, a polysome profile analysis was performed on yeast strains expressing tr-4EBP2, cLIPS2^{AA}, and cLIPS2. Polysome profiling is often used to study global translation by taking a snapshot of the number of translating ribosomes on all mRNA in an organism.[72] In this technique, cell lysate is sedimented through a sucrose gradient that separates mRNA based on the number of ribosomes associated. The ratio of mRNA-ribosome complexes, or polysomes, to ribosomes not associated with mRNA, or monosomes, (the P/M ratio) is indicative of translational status. If translation initiation is defective, fewer ribosomes are

loaded onto mRNA, decreasing polysome abundance and increasing monosome abundance.[73, 74]

Polysome profiling analysis of Jo56 yeast expressing cLIPS2^{AA} in the dark gave a P/M ratio of about 1.2 ± 0.2 whereas yeast expressing tr-4EBP2 exhibited a markedly decreased P/M of 0.5 ± 0.1 (Figure 7B). This decrease in P/M ratio indicates a substantial reduction in translation initiation in the presence of an active 4EBP2 construct. The P/M ratio of cLIPS2 (0.5 ±0.1) in the dark also indicates substantial inhibition of translation initiation. The low P/M ratio of cLIPS2 in the dark is consistent with the observation that cLIPS2 in the dark also slows the growth rate significantly compared to cLIPS2^{AA} (Fig. 6, Supplementary Fig. 5). The further 35 ± 5% decrease in growth rate observed with cLIPS2 in the light (Fig. 6), might be expected to cause a further decrease in P/M ratio to approximately 0.35 (see Supplementary Fig. 5). The observed average P/M ratio for cLIPS2 in the light was 0.4 ± 0.1 (Figure 7B) but variability between polysome profiling runs done on different days (error bars in Figure 7B) means that this small additional effect on the P/M ratio cannot be reliably measured under these conditions.

The substantial effect of dark-adapted cLIPS2 on translation initiation indicates that significant binding to eIF4E occurs in the dark. In this system, the level of expression of cLIPS2 cannot be controlled, and may vary as a function of the stage of the growth curve (polysome profiles were analyzed at early log phase). As noted above, Western blot analysis indicates that there may also be feedback effects where active cLIPS2 proteins inhibit their own synthesis.

Effect on translation in vitro

To directly control the concentration of cLIPS constructs, we expressed and purified cLIPS1, cLIPS2 and the corresponding cLIPS1^{AA} and cLIPS2^{AA} controls (Fig. S6), and tested their ability to inhibit translation in a cell-free assay prepared from lysates of the Jo56 strain. We used mRNA coding for *Renilla* luciferase that was either capped or contained an internal ribosome entry site (IRES) (Fig. S7). Translation of IRES-containing mRNA does not require eIF4E and thus serves as a further test of the mechanism of inhibition in this system. These mRNAs were added to lysates and the luminescence of the translated *Renilla* luciferase was used to measure the rate of translation.

In the Jo56 lysates, cLIPS1 and cLIPS2 showed clear inhibition of translation of capped mRNA transcripts under blue light compared to the dark (Figure 8A). For cLIPS1, translation was inhibited more strongly in the light at higher protein concentrations, while for cLIPS2, there was a clear difference between light and dark with even 0.5 pmol of protein added (Figure 8A). These results are consistent with the growth assay results where cLIPS2 showed a larger difference in inhibition between the light- and dark-state. The negative controls, cLIPS1^{AA} and cLIPS2^{AA}, did not affect translation under either dark or light conditions. Full-length 4EBP2 inhibited translation strongly with no difference between light and dark.

To test the cap-dependence of the system, we examined translation of *Renilla* luciferase encoded by uncapped mRNA containing an IRES. We used the IRES from yeast poly-A

binding protein (PAB1) mRNA.[75] PAB1 has been proposed to bind to this IRES and recruit eIF4G to the 5' end of the transcript, initiating translation.[75] When full-length 4EBP2 was added to lysates with IRES-dependent mRNA, an increase in translation was observed (Figure 8B). We hypothesize that eIF4E is competing with PAB1 for binding to eIF4G in the lysate; when 4EBP2 binds to eIF4E, eIF4G is then free to bind with PAB1, thereby increasing IRES-dependent translation.

When cLIPS1 or cLIPS2 was added to lysates with PAB1 IRES-dependent transcripts, the rate of *Renilla* luciferase translation increased somewhat in the dark but increased substantially upon irradiation (Figure 8B). cLIPS1 showed a smaller increase in translation upon irradiation than cLIPS2, but less dark inhibitory activity than cLIPS2. At high concentrations, cLIPS2 appears to impact translation both in the dark and the light, consistent with the behaviour observed in the yeast growth and polysome assays. The controls cLIPS1^{AA} and cLIPS2^{AA} showed no effect on translation either in the light or the dark.

cLIPS binding to eIF4E in vitro

Having demonstrated that cLIPS constructs can cause light-dependent inhibition of cap-dependent translation, we wished to directly confirm whether the mechanism of this inhibition was via light-dependent binding to eIF4E. For *in vitro* tests, cLIPS1, cLIPS1^{AA}, and human eIF4E with a GB1-tag (GB1-eIF4E) were expressed and purified (Fig. S6). Photoswitching and thermal recovery of the purified cLIPS protein was confirmed using UV-Vis spectroscopy (Figure 9A). The half-life for thermal recovery of cLIPS1 and cLIPS1^{AA} was measured at 3 min, a typical value for the AsLOV2 domain in these constructs (Figure 9B).[76]

The interaction between the cLIPS constructs and GB1–4E was then analyzed by size-exclusion chromatography (SEC). Alone, cLIPS1 constructs eluted as single peaks at 14.5 mL (Fig. S8). This elution volume did not shift significantly when the proteins were irradiated with blue light (Fig. S8). GB1–4E also eluted as a single peak around 13 mL (Fig. S8). When the control construct cLIPS1^{AA} was mixed with GB1-eIF4E and injected (10 μM each), two peaks were eluted, one at the retention volume of cLIPS alone and one at the retention volume of GB1-eIF4E alone, indicating the proteins do not interact under these conditions. No difference was seen in this elution pattern upon blue light irradiation (Figure 9C, right chromatograph). When dark-adapted cLIPS1 was mixed with GB1–4E (10 μM each) and injected onto the column a similar pattern was seen (Figure 9C, left chromatograph) indicating little interaction between the proteins. In contrast, under constant blue light irradiation, the first peak eluted much earlier and contained more material than the second peak. This indicates that a complex is formed between cLIPS1 and GB1–4E in the light. Eluted light-state and dark-state cLIPS1 + GB1–4E were collected and analyzed by SDS-PAGE. Under blue light, cLIPS1 co-elutes with GB1–4E whereas it elutes separately in the dark (Figure 9C, left panel).

A similar analysis was performed on cLIPS2 mixed with GB1–4E (Fig. S9). In this case, when dark-adapted cLIPS2 was mixed with GB1–4E, at the concentrations required for SEC, a single broad peak eluted from the column consistent with weak, dynamic binding

between cLIPS2 and GB1–4E in the dark. However, under blue light, the chromatograph showed the elution of another peak, much earlier than the single peak seen in the dark, consistent with the formation of a tightly bound complex between cLIPS2 and GB1–4E. As before, eluted light-state and dark-state cLIPS2 + GB1–4E were collected and analyzed by SDS-PAGE. While in the dark, cLIPS2 low amounts of cLIPS2 co-elute with GB1–4E over most fractions, in the light, most of the cLIPS2 is observed to co-elute with GB1–4E much earlier, again consistent with formation of a tight complex between cLIPS2 with GB1–4E in the light (Fig. S9).

Discussion

Translation is a fundamental cellular process and is the primary determinant of protein abundance in a cell.[77] There has been growing interest in determining the role of translation regulation in diverse settings; however, it remains difficult to control translation with spatiotemporal precision.[6, 78, 79] An optogenetic tool with a defined mechanism of action on the endogenous translational machinery would enable analysis of systems where a high degree of spatiotemporal resolution is important. For example, local translation at synapses is important for memory formation and retrieval,[80] and aberrant eIF4E-dependent translation has been linked to neurological diseases such as Fragile X syndrome and autism spectrum disorders.[81]

The yeast-based system described here provides a means for quickly screening a library of constructs for effects on human 4E-mediated translation *in vivo*. We have shown that 4EBP constructs that inhibit growth in this system are doing so by inhibiting translation initiation via direct binding to human eIF4E. This approach is suitable not only for constructs with 4EBP inserts but also variants of other regulators that target eIF4E.

The system could be further modified to permit better control of expression levels of opto-4EBPs. For example, in the current GAL promoter based system, transcription rates are not tunable, and overexpression is expected to decrease light/dark differences observed. This may be circumvented by using tunable yeast expression systems.[82, 83] Selection for strong eIF4E binding under low expression conditions in the light, combined with selection for weak or no eIF4E binding under high expression conditions in the dark could lead to opto-4EBPs with greatly improved dynamic range. A second issue is that active 4EBP constructs may be repressing their own (cap-dependent) translation (Fig. S4), again leading to decreased light/dark differences. This could be circumvented by having the opto-4EBP constructs produced from IRES-containing mRNAs.[84] Most importantly, by linking optogenetic function to growth in a well-characterized model system, high throughput approaches for generating large defined libraries together with next-generation sequencing can be readily employed to discover improved optogenetic tools.[85]

Using the current system, we identified cLIPS1 and cLIPS2, two light-activated 4EBP2 constructs, capable of binding human eIF4E *in vitro* and downregulating translation initiation in yeast expressing human 4E. These constructs thus have the essential requirements to enable light-dependent control of translation in other settings. How they function in other settings, however, will necessarily depend on what other protein factors are

present. More complex cell types use more complex regulatory networks of proteins that can compete with 4EBPs for eIF4E binding. In yeast, only four proteins have been shown to directly interact with eIF4E – eIF4G1, eIF4G2, Eap1 (required for mRNA degradation), and p20/CAF20 (a translational regulator).[86] In metazoa, numerous additional eIF4E binding proteins have been identified[87, 88] including 4E-T and CYFIP1, Angel1[89], and others yet to be characterized.[90]

The effect of light-dependent translation inhibition by cLIPS constructs in different cell types must, therefore, be analyzed under carefully defined conditions. For example, a constitutively active (non phosphorylatable) version of 4EBP1 does not affect basal translation in mouse thymocytes, but dramatically inhibits the increased translation seen with hyperactivation of the oncogenic kinase Akt, greatly slowing lymphomagenesis.[91] Likewise, Benson and colleagues found that expression of a constitutively active 4EBP had negligible effects on global translation in PC12 cells, but dramatic effects on translation-dependent processes in axonal growth cones.[84]

In addition, as noted above, introduction of opto-4EBPs are likely to produce homeostatic responses, for example up-regulation of active eIF4E or redistribution of eIF4Es between nuclear, cytoplasmic, and/or RNA granules (P-bodies and stress granule) locations.[44, 45] Finally, regulation of eIF4E activity can differentially regulate the translation of subsets of mRNAs under different conditions and in different cell types.[36, 92] Given the complexity of translational regulatory mechanisms, the possible responses of cells to opto-4EBPs are numerous. We anticipate that tools such as cLIPS and improved variants are precisely what is required to help dissect the molecular events underlying dynamic translational responses.

Lastly, from the standpoint of protein engineering, this work introduces a unique variant of the *Avena Sativa* LOV2 scaffold for the design of optogenetic constructs. We have shown that the insertion of an intrinsically disordered peptide sequence between the C-terminal Jα-helix and N-terminal A'α-helix of AsLOV2 together with the creation of new N- and C-termini between the Hβ and Iβ strands results in a stable folded protein capable of photoactivation. Since the Jα and A'α helices are the regions of AsLOV2 that undergo the largest changes in conformation upon photoactivation, this circularly permutation of AsLOV2 may prove generally useful. Simply masking the 4EBP2 binding site via fusion the C-terminal end of the J-α helix in wild-type AsLOV2,[53] was not able to produce light-switchable activity in the present case.

Methods

Cloning

Genes for the rationally designed panel of opto-4EBPs were synthesized and cloned into the pET24b vector with a C-terminal 6xHis-tag by Biobasic. To construct the yeast expression plasmids, opto-4EBP genes were amplified from their respective pET24b plasmids using the polymerase chain reaction (PCR) and ligated into a pRS316 vector under the GAL1 promoter using Gibson Assembly Master Mix (New England Biolabs E2611S) or NEBuilder HiFi Assembly Master Mix (New England Biolabs E2621S). The pRS316 plasmid with

GAL1 promoter was generously given to us by Benjamin Scott from the Peisajovich lab (Univ. Toronto).

For controls, site-directed mutagenesis on cLIPS1, and cLIPS2 for the construction of cLIPS1^{AA}, cLIPS1^{Y46A}, cLIPS1^{Y46F}, and cLIPS2^{AA} was performed using the Q5 Site-Directed Mutagenesis Kit (New England Biolabs). To construct the yeast expression plasmid containing truncated 4EBP2, the 4EBP2 fragment of cLIPS1 was amplified by PCR and ligated into pRS316 using Gibson assembly. To construct the yeast expression plasmid of full-length wild-type 4EBP2, the gene was amplified from a pET-Sumo plasmid encoding wild-type 4EBP2, generously given to us by Alaji Bah from the Forman-Kay lab (Hospital for Sick Children, Toronto).

To add a C-terminal myc tag onto select constructs (cLIPS1, cLIPS1^{AA}, cLIPS2, cLIPS2^{AA}, tr-4EBP2, wt-4EBP2, and AsLOV2), the pRS316 plasmids with the non-myc-tagged versions were amplified using primers encoding a short GSG linker, the myc sequence (EQKLISEEDL), and a stop codon. These were then assembled with the Q5 Site-Directed Mutagenesis Kit (New England Biolabs). The sequences of all constructs are shown in Figure S1.

Library construction

For the primer-based PCR library, a set of four primers (three forward and one reverse) was added into a single PCR with Q5 polymerase (NEB) and the pRS316 (cLIPS1) template. The binding sites of the three forward primers were staggered from amino acids 78–80 (EFL). The library was intended to sample shorter linker lengths between the C-terminal end of the tr-4EBP2 insert and the N-terminal end of AsLOV2 in cLIPS1. The resultant PCR was ligated with the Q5 Site-Directed Mutagenesis Kit (New England Biolabs), then transformed into Jo56 yeast cells and DH5α bacterial cells. The transformed Jo56 were replica-plated on two identical SC-W-U+Gal plates (see growth assays section below for details on media). One was grown in the light, while one was grown in the dark. Colonies with less growth in the light were lysed, and sequenced. The library quality was assessed from the transformed DH5α *E. coli* cells.

For the error-prone PCR library, the cLIPS2 insert was amplified with a PCR mix containing the following: 1 μL Taq polymerase (New England Biolabs M0267S), 10 μL 10X ThermoPol reaction buffer, 2 μL 50X dNTP mix (Thermo Fisher Scientific R0191), 5.5 mM $MgCl_2$, 5.5 mM $MnCl_2$, 5 μM forward primer, 5 μM reverse primer, and 10 ng pRS316 (cLIPS2) template. The forward primer amplified cLIPS2 from residue 16 and the reverse primer amplified cLIPS2 from residue 104 (see sequences Figure S1). The pRS316 (cLIPS2) vector was amplified with Q5 polymerase (NEB). The vector and insert were assembled using NEBuilder HiFi Assembly Master Mix (New England Biolabs E2621S) according to the manufacturer's instructions. Afterwards, 5 μL was transformed into *E. coli* DH5-α for amplification and sequencing, and into Jo56 using the Fast Yeast Transformation kit (G-Biosciences). Sanger sequencing indicated an error rate of 2–5 nucleotides per kilobase. After 3 nights of growth at 30°C, Jo56 were replica plated onto two SC-W-U+Gal plates. As with the primer-based PCR library, one was grown in the light, while the other was grown in

the dark. Colonies with less growth in the light were picked, lysed and sequenced. Only small test libraries of <5000 colonies were screened.

Yeast growth assay

The Jo56 strain (MATα cdc33-Δ::LEU2 leu2 ura3 his3 trp1 ade2 [YCpTrp-Hu4E TRP1]) was generously given to us by the McCarthy lab (U. Warwick). Yeast cells were transformed with pRS316 plasmids using the Fast Yeast Transformation kit (G-Biosciences). Yeast were plated on agar plates with synthetic complete selective media, composed of 2 g/L Drop-out Medium Supplement without histidine, leucine, tryptophan and uracil (Bioshop DOM003.100), 1.7 g/L Yeast Nitrogen Base (Biobasic Canada S505), 5 g/L ammonium sulfate (Bioshop AMP302.1), 50 mg/L L-histidine (Bioshop HIS100.10), 100 mg/L L-leucine (Bioshop LEU222.25), 100 mg/L adenine sulfate (ADS201.5), and either 2% glucose (SC-W-U+Glu), 2% galactose (SC-W-U+Gal) or 2% raffinose (SC-W-U+Raf). For glycerol stocks, single colonies were picked from plates and stored in SC-W-U+Glu media containing 15% glycerol at −80°C.

Transformed yeast from glycerol stocks were streaked onto SC-W-U+Glu agar plates and grown at 30°C for 2 days. A single colony was picked and grown in SC-W-U+Glu media overnight at 30°C. One mL of culture was then centrifuged at 500 rpm, washed with water, and SC-W-U+Gal media. The cells were diluted to an OD (optical density) of 0.4 and serially diluted in a 96-well plate. On two identical SC-W-U+Gal agar plates, 5μL of each dilution was spotted. One plate was placed under a 450 nm LED array at 0.23–0.25 mW/cm^2. The other plate was wrapped in foil. Both plates were then incubated for 64 hours at 30°C.

Growth curves in liquid culture

Yeast cells were first streaked onto SC-W-U+Glu plates from glycerol stocks and grown for 2 nights. Colonies were picked and grown overnight at 30°C in 10 mL SC-W-U+Glu liquid cultures. Then, 1 mL of the cultures was pelleted and washed in SC-W-U+Raf and diluted to an OD of 0.05–0.09 in 125 mL SC-W-U+Raf media. These cultures were grown for 65 hours at 25°C.

To measure growth, yeast cells were diluted to OD = 0.06 in SC-W-U+Gal. In a 96-well plate, 300 μL of culture was added to each well. A Breathe-Easy sealing membrane (Sigma-Aldrich Z380059) was applied to the plate. The plate was then incubated at 30°C with shaking in an automated shaker and platereader made by S&P Robotics. OD readings of the plate were checked every 15 min. For growth curves under blue light, an intensity of 0.06 mW/cm^2 was used.

The doubling time (D) was calculated according to St. Onge et al.[69] Here, an arbitrary final OD (OD_f) at mid-log phase was chosen. The initial OD (OD_i) was determined by dividing OD_f by 8 (or 3 doublings). The doubling time was calculated as the difference between the time the culture reached OD_f (t_f) and the time that the culture reached OD_i (t_i) divided by the number of generations:

$$D = \frac{t_f - t_i}{3}$$

Polysome assays

A modified version of a protocol described by Pospisek and Valásek[73] was employed. Yeast cells were streaked from glycerol stocks and single colonies were grown overnight in 10 mL of SC-W-U+Glu. The overnight culture was then diluted from an OD_{600} of 8.0–10.0 to 0.05–0.08 in 40 mL of SC-W-U+Raf media. This culture was grown in a 125 mL Erlenmeyer flask for 65–72 hours. Cells were then diluted to an OD_{600} of 0.04–0.05 in a 1 L Erlenmeyer flask with 200 mL of SC-W-U+Gal media. These were grown under either light or dark conditions for 18–22 hours in a shaking incubator at 30°C and 200 rpm. For the light samples, a 447 nm blue light array (0.09 mW/cm^2) flashing 30 s on and 30 s off was used. Dark samples were wrapped with aluminum foil and grown in the same incubator. Cultures were started at staggered time points (based on a previously determined doubling time) so all strains reached an OD_{600} of 1.0–1.1 simultaneously. At the OD_{600} of 1.0–1.1, cells were incubated at 30°C for 20 min with 100 μg/mL of cycloheximide. For myc-tagged constructs, samples were taken at this point and frozen at −80°C (without cycloheximide) for analysis by western blot. Cells were lysed as described[73] in 0.02% diethyl pyrocarbonate in lysis buffer (20 mM Tris HCl, pH=7.4, 50 mM KCl, 10 mM $MgCl_2$, 1 mM DTT). A Gradient Master (BioComp) was used to make sucrose gradients (4.5–45%). These gradients were prepared with lysis buffer the night before ultracentrifugation and kept at 4°C. Lysates were quantified using a NanoDrop 1000 (Thermo Fisher Scientific) and normalized according to the absorbance at 260 nm in 300 μL freshly prepared lysis buffer. After dilution, 200 μL of the lysate was loaded on top of the sucrose gradient. These gradients were centrifuged in a Beckman L-80 ultracentrifuge at 36000 rpm in a SW41-Ti rotor for 3 h at 4°C. These gradients were passed through a detector (Isco UA-6 UV/VIS) using 60% (w/v) sucrose in water at a flow rate of 900 μl/min using a peristaltic pump (Teledyne ISCO). A PowerChrom 280 digitizer was used to record the polysome profile and the multipeak fitting routine in Igor Pro 7 was used to determine the polysome to monosome ratios.

Western blot analysis

Yeast cells were grown as described as for polysome assays. Lysates were prepared as described by Zhang *et al*[93] An equal volume (10 μL) of each sample was loaded in a 10% TGX stain-free SDS-PAGE gel (Bio-Rad 161–0183). Proteins were transferred using the Trans-Blot Turbo Transfer System (Bio-Rad 1704150) and ready-to-assemble transfer kits (Bio-Rad 1704273). The manufacturer recommended time (3 min) was used for transfer.

The membrane was blocked overnight at 4°C in tris-buffered saline with 20% Tween-20 (TBST) and 5% skim milk (Bioshop SKI400.500). A primary rabbit anti-myc-tag polyclonal antibody (PA1–981) and a primary mouse anti-GAPDH antibody dilution (1:5000) were prepared in TBST with 5% skim milk. The membrane was incubated in both primary rabbit and mouse antibody simultaneously for an hour at room temperature. The membrane was washed 3 times in TBST for 5 min each. The membrane was then incubated at room temperature for an hour with a secondary rabbit and mouse HRP antibody simultaneously

(1:5000 dilution) in TBST. A Bio-Rad Gel Doc System was used to image the membrane after 3 washes in TBST for 5 minutes each.

Yeast extract preparation

Yeast lysates were prepared according to a protocol from Iizuka *et al*[94] with modifications described below: From glycerol stocks, Jo56 were streaked onto plates with YPD media (20 g/L Peptone, 10 g/L Yeast Extract and 2% glucose). A single colony was picked and grown in 10 mL of YPD media overnight at 30°C. Enough cells were added into 1L YPD media to reach an OD of 2.0 in 20 hr at 30°C. Cells were harvested at mid-log phase (OD = 2.0), washed with distilled water and 150 mM HEPES-KOH pH7,4, 500 mM potassium acetate, 10 mM magnesium acetate, 2 mM DTT, 100 μM PMSF, 7% mannitol (Buffer ADPM). Cells were resuspended in 250–500 μL Buffer ADPM and pipetted into liquid nitrogen to form 'pellets' which were stored at −80°C.

For cell lysis, pellets were ground vigorously with liquid nitrogen in a mortar and pestle. During grinding, liquid nitrogen was added 2–3 times and care was taken not to allow the cells to thaw. The final homogenous powder was collected in tubes and thawed on ice. The lysate was spun down in a microfuge for 10 min at 13000 rpm to remove insoluble material. The supernatant was immediately separated from the insoluble fraction and applied to a G-25 superfine size-exclusion column pre-equilibrated with 150 mM HEPES-KOH pH 7,4, 500 mM potassium acetate, 10 mM magnesium acetate, 2 mM DTT, 100 μM PMSF (Buffer ADP) at 4°C. Fractions of about 200 μL were collected and the absorbance at 260 nm (A_{260}) was measured. Fractions with high A_{260} (>80 Units/mL) were tested for activity in an *in vitro* translation assay (see below). The most active fractions were pooled, aliquoted and flash frozen with liquid nitrogen. These were stored at −80°C.

Synthesis of mRNA.

Two plasmids, 1762 (cap dependent) and 1833 (cap independent), encoding Renilla luciferase were linearized with Xho1 (NEB R0146S) (10 μg of plasmid were digested with 1 μL enzyme in 50 μL reaction mix at 37°C). After 1.5 hours, an additional 1 μL enzyme was added and the reaction was incubated for a further 1 hour. DNA was purified with GeneJET PCR Purification Kits (Thermo Fisher K0701) and added to a reaction mix with T3 DNA polymerase (Thermo Fisher Scientific EP0101) according to the manufacturer's protocol to produce RNA.

The transcription product was treated with RNase-free DNase I (NEB M0303S), (5 μL were added to each polymerase reaction and incubated at 37°C for 20 minutes), to remove the template. RNA was purified by phenol-chloroform extraction. Briefly, the sample volume was increased to 200 μL with TE (10 mM Tris, 1 mM EDTA) pH 7.0, an equal volume of phenol:chloroform:isoamyl alcohol (Bioshop PHE512.100) was added and the suspension was vortexed for 15 seconds and centrifuged for 5 minutes to isolate the upper phase. The extraction was repeated and the upper phases pooled. The RNA was precipitated with ammonium acetate (an equal volume of 5 M ammonium acetate was added, the sample was incubated overnight at −20°C and centrifuged in a microfuge for 30 minutes at 14K. The

pellet was rinsed with ice-cold 70% ethanol, dried and dissolved in 50 μL RNase-free water).

RNA from plasmid 1762 was capped (Cap 0, *i.e.* without the addition of a methyl group at the 2'-O position of the penultimate nucleotide of the transcript) using ScriptCap™ m^7G Capping System (CELLSCRIPT™ C-SCCE0625). The capped RNA was purified by phenol-chloroform extraction and ammonium acetate precipitation as described above. RNA from both plasmids was finally purified using GeneJET RNA Purification Kits (Thermo Fisher Scientific K0731), quantified using A_{260} on a Nanodrop 1000 (Thermo Fisher Scientific) and analysed by agarose electrophoresis using the method of Masek *et al.*[95]. RNA was aliquoted and stored at −80°C.

In vitro translation assay

All proteins (purified as described below) were buffer-exchanged a day beforehand into 20 mM HEPES-KOH pH 7.4, 50 mM NaCl and 1 mM fresh DTT. On the day of an experiment, all proteins were diluted to 2 μM and kept on ice in the dark for the duration. The mRNA was diluted to 30 ng/μL on the day of the experiment and also kept on ice for the duration. Light/dark experiments on the same protein were done concurrently and every point in the protein titration was prepared in triplicate.

The translation reactions were prepared according to the protocol from Iizuka *et al.*[94] with slight modifications as described below: The total volume of each reaction was 5 μL and was prepared in thin-walled 0.2 mL tubes pre-chilled in ice-water. A pre-mix was assembled on ice with the following components per reaction: 1.5 μL yeast extract, 1.55 μg creatine phosphokinase (Roche SKU 10127566001), 1.2 Units RNasin Plus RNase Inhibitor (Promega SKU N2611), 30 ng mRNA, and 1.04 μL of an amino acid cocktail. The amino acid cocktail contained 132 mM HEPES-KOH pH 7.4, 720 mM potassium acetate, 9 mM magnesium acetate, 4.5 mM ATP, 0.6 mM GTP, 150 mM creatine phosphate (Roche SKU 10621714001), 0.24 mM 20 amino acid mix (Promega SKU L4461), and 10.2 mM DTT.

In the dark, the pre-mix was split into 4 equal aliquots of 24 μL . Each aliquot was enough for 6 reactions at each protein concentration (0 μM, 0.1 μM, 0.2 μM, 0.4 μM). Then, in the dark, protein aliquots with working stock concentrations of 2 μM, 1 μM and 0.5 μM were prepared. In each 24 μL pre-mix aliquot, 6 μL of the respective protein stock was added. Buffer was added to the pre-mix aliquot prepared for 0 μM protein. To assemble the final reaction, these pre-mixes with protein or buffer were aliquoted into pre-chilled reaction tubes at 5 μL per reaction. Three reactions per protein concentration (12 samples) were incubated in ice water in the dark for 10 min (dark samples). The remaining 12 samples (light samples) were flashed with blue light (50 $\mu W/cm^2$) 10 s on and 10 s off for 30 s (off-times were kept in ice water to prevent the reaction from starting). The light samples were placed over a 50 $\mu W/cm^2$ blue light (447 nm) in a 25°C water bath. The dark samples were incubated over the same blue light but in a separate 25°C water bath wrapped in foil. All samples were then incubated concurrently for 40min.

Renilla luciferase substrate and passive lysis buffer (PLB) from the Promega Renilla Luciferase Assay System (SKU E2820) were prepared according to the manufacturer's

instructions. For each translation reaction, 10 μL PLB was added into a polystyrene tube (Falcon SKU 352052). After incubation, samples were immediately placed in ice water and prepared for luminometer readings. In each tube with PLB, 2 μL of the translation reaction was added. Then, 50 μL of the Renilla luciferase substrate was added and pipetted 6 times before the tube was placed in the luminometer (Berthold Sirius Single Tube Luminometer). Luminescence was read for 10 s after a 10 s delay.

Protein purification

E. coli BL21 (DE3) cells were transformed by heat-shock and incubated on agar plates containing 25 g/L Luria Broth (LB) (Bioshop LBL407.1) and 50 μg/mL kanamycin (Bioshop KAN201.10) overnight at 37°C. Single colonies were grown in 25 mL LB with 50 μg/mL kanamycin overnight at 37°C. The 25 mL cultures were added into 1 L LB with 50 μg/mL kanamycin and grown until OD_{600}=0.6–0.8. Cultures were then induced with 500 μM IPTG and incubated overnight (~20 h) with shaking in the dark at 17°C. Cells were collected by centrifugation and stored at −20C.

For purification of cLIPS1, cLIPS2 and derivatives, cells were resuspended and sonicated in lysis buffer containing 40 mM Tris (pH 8), 300 mM NaCl, and 0.15 mM DTT. Insoluble debris was removed with centrifugation and the soluble fraction was filtered through a 0.45 μm filter and added onto 1–4 mL of Ni-NTA in a Glass Econo-Column (Bio-Rad). The column was washed with 50 mL of lysis buffer, then 25 mL of lysis buffer supplemented with 2 M NaCl, and finally 25 mL lysis buffer with 5 mM imidazole. Yellow protein was eluted by lysis buffer supplemented with 200 mM imidazole. The eluant was dialysed overnight at 4°C against 40 mM Tris-acetate, 1 mM EDTA, 100 mM NaCl, and 0.15 mM DTT (dialysis buffer). After 2–3 buffer exchanges, proteins were concentrated by Amicon centrifugal filters and further purified on a Superdex™ 75 10/300 GL size exclusion (SEC) fast protein liquid chromatography (FPLC) column, pre-equilibrated with the dialysis buffer supplemented with 0.02% NaN_3. The fractions with the highest 447 nm absorbance contained the desired proteins as confirmed with ESI-MS (Figure S3). The absorbance of each fraction was then separately measured by UV-Vis and those with a A447/280 ratio of 0.27 or higher were pooled.

The purification of GB1–4E was carried out in the same manner as for the purification of cLIPS constructs except the lysis buffer used was 50 mM sodium phosphate (pH 6.5), 300 mM NaCl, and 1 mM DTT. The dialysis buffer was 50 mM sodium phosphate (pH 6.5), 100 mM NaCl and 1 mM DTT (with 0.02% NaN_3 for SEC-FPLC). Due to its instability, experiments requiring GB1–4E were performed within two days of SEC purification.[96] Wild-type 4EBP2 protein was a generous gift given to us by Alaji Bah from the Forman-Kay lab.

UV-Vis characterization

All characterization was performed in GB1–4E dialysis buffer: 50 mM sodium phosphate (pH 6.5), 100 mM NaCl, and 1 mM DTT. All versions of cLIPS were either buffer exchanged by Amicon centrifugal filters or SEC. Spectra for all cLIPS proteins were obtained at a concentration of ~5 μM. To examine the photocycle, cLIPS proteins were

irradiated in a quartz cuvette for 1 min with a 450 nm LED (>10 mW/cm^2). After turning off the LED, scans were obtained at 480 nm/sec every 40s. To calculate the half-life of thermal relaxation, the absorbance at 446 was plotted versus time. The data were then fit to an exponential function to obtain the rate constant.

SEC analysis of cLIPS/eIF4E interactions

Analytical SEC was performed on a Superdex™ 75 10/300 GL column that was pre-equilibrated with 50 mM sodium phosphate (pH 6.5), 100 mM NaCl, 1 mM DTT and 0.02% NaN_3. The flow-rate was 0.5 mL/min. All proteins were exchanged into this buffer prior to the SEC binding experiments. For full dark-adaptation, stock solutions of cLIPS were kept in the dark on ice for 10 min prior to the SEC binding experiment. From the dark-adapted stock solution in the dark, a cLIPS protein was mixed with GB1–4E. The final concentration for both proteins was 10 μM and the final volume was 400 μL. The mixture was equilibrated at room temperature for 10 min before injection onto the column. For light-state samples, the cLIPS protein was first mixed with GB1–4E in the dark. The mixture was then equilibrated for 10 min at room temperature in the dark. Before injection, the sample was placed under a blue light LED array (447nm) at 0.6 mW/cm^2 for 1 min before immediate injection onto the column. In the light-state SEC experiments, a blue light LED array was placed next to the column so that samples were continuously irradiated with a light intensity of 0.2–0.6 mW/cm^2.

Supplementary Material

Refer to Web version on PubMed Central for supplementary material.

Acknowledgements.

We would like to acknowledge helpful discussions with Helena Friesen from Brenda Andrews' lab, University of Toronto, and assistance from Ryan Woloschuk with the characterization of PYP-based constructs.

This work has been supported by the NIH.

References:

1. Sesma A, Castresana C, and Castellano MM (2017) Regulation of Translation by TOR, eIF4E and eIF2alpha in Plants: Current Knowledge, Challenges and Future Perspectives, Front. Plant Sci 8, 644. [PubMed: 28491073]
2. Martin KC, and Ephrussi A (2009) mRNA localization: gene expression in the spatial dimension, Cell 136, 719–730. [PubMed: 19239891]
3. Ma XM, and Blenis J (2009) Molecular mechanisms of mTOR-mediated translational control, Nat. Rev. Mol. Cell. Biol 10, 307–318. [PubMed: 19339977]
4. Sengupta S, Peterson TR, and Sabatini DM (2010) Regulation of the mTOR complex 1 pathway by nutrients, growth factors, and stress, Mol. Cell 40, 310–322. [PubMed: 20965424]
5. Santini E, Huynh TN, and Klann E (2014) Mechanisms of translation control underlying long-lasting synaptic plasticity and the consolidation of long-term memory, Prog. Mol. Biol. Transl. Sci 122, 131–167. [PubMed: 24484700]
6. Rosenberg T, Gal-Ben-Ari S, Dieterich DC, Kreutz MR, Ziv NE, Gundelfinger ED, and Rosenblum K (2014) The roles of protein expression in synaptic plasticity and memory consolidation, Front. Mol. Neurosci 7, 86. [PubMed: 25429258]

7. Martin KC, and Zukin RS (2006) RNA trafficking and local protein synthesis in dendrites: an overview, J. Neurosci 26, 7131–7134. [PubMed: 16822966]
8. Chasse H, Aubert J, Boulben S, Le Corguille G, Corre E, Cormier P, and Morales J (2018) Translatome analysis at the egg-to-embryo transition in sea urchin, Nucleic Acids Res 46, 4607–4621. [PubMed: 29660001]
9. Penrod RD, Wells AM, Carlezon WA Jr., and Cowan CW (2015) Use of adeno-associated and Herpes simplex viral vectors for in vivo neuronal expression in mice, Curr. Protoc. Neurosci 73, 4 37 31–31.
10. Naqib F, Farah CA, Pack CC, and Sossin WS (2011) The rates of protein synthesis and degradation account for the differential response of neurons to spaced and massed training protocols, PLoS Comput. Biol 7, e1002324. [PubMed: 22219722]
11. Cagnetta R, Frese CK, Shigeoka T, Krijgsveld J, and Holt CE (2018) Rapid cue-specific remodeling of the nascent axonal proteome, Neuron 99, 1–18. [PubMed: 30001504]
12. Repina NA, Rosenbloom A, Mukherjee A, Schaffer DV, and Kane RS (2017) At light speed: Advances in optogenetic systems for regulating cell signaling and behavior, Annu. Rev. Chem. Biomol. Eng 8, 13–39. [PubMed: 28592174]
13. Rost BR, Schneider-Warme F, Schmitz D, and Hegemann P (2017) Optogenetic tools for subcellular applications in neuroscience, Neuron 96, 572–603. [PubMed: 29096074]
14. Ando H, Furuta T, Tsien RY, and Okamoto H (2001) Photo-mediated gene activation using caged RNA/DNA in zebrafish embryos, Nat. Genet 28, 317–325. [PubMed: 11479592]
15. Zhang D, Zhou C, Busby K, Alexander S, and Devaraj NK (2018) Light-activated control of translation by enzymatic covalent mRNA labeling, Angew. Chem. Int. Ed. Engl
16. Shestopalov IA, Sinha S, and Chen JK (2007) Light-controlled gene silencing in zebrafish embryos, Nat. Chem. Biol 3, 650–651. [PubMed: 17717538]
17. Mikat V, and Heckel A (2007) Light-dependent RNA interference with nucleobase-caged siRNAs, RNA 13, 2341–2347. [PubMed: 17951332]
18. Govan JM, Young DD, Lusic H, Liu Q, Lively MO, and Deiters A (2013) Optochemical control of RNA interference in mammalian cells, Nucleic Acids Res. 41, 10518–10528. [PubMed: 24021631]
19. Connelly CM, Uprety R, Hemphill J, and Deiters A (2012) Spatiotemporal control of microRNA function using light-activated antagomirs, Mol. Biosyst 8, 2987–2993. [PubMed: 22945263]
20. Goard M, Aakalu G, Fedoryak OD, Quinonez C, St Julien J, Poteet SJ, Schuman EM, and Dore TM (2005) Light-mediated inhibition of protein synthesis, Chem. Biol 12, 685–693. [PubMed: 15975514]
21. Sadovski O, Jaikaran AS, Samanta S, Fabian MR, Dowling RJ, Sonenberg N, and Woolley GA (2010) A collection of caged compounds for probing roles of local translation in neurobiology, Bioorg. Med. Chem 18, 7746–7752. [PubMed: 20427189]
22. Marter K, Wetzel J, Eichhorst J, Eremina N, Leboulle G, Barth A, Wiesner B, and Eisenhardt D (2017) Inhibition of protein synthesis with highly soluble caged compounds, Chemistryselect 2, 6212–6217.
23. Buhr F, Kohl-Landgraf J, tom Dieck S, Hanus C, Chatterjee D, Hegelein A, Schuman EM, Wachtveitl J, and Schwalbe H (2015) Design of photocaged puromycin for nascent polypeptide release and spatiotemporal monitoring of translation, Angew. Chem. Int. Ed. Engl 54, 3717–3721. [PubMed: 25656536]
24. Ogasawara S (2014) Control of cellular function by reversible photoregulation of translation, Chembiochem 15, 2652–2655. [PubMed: 25351829]
25. Cao J, Arha M, Sudrik C, Bugaj LJ, Schaffer DV, and Kane RS (2013) Light-inducible activation of target mRNA translation in mammalian cells, Chem. Commun. (Camb.) 49, 8338–8340. [PubMed: 23925486]
26. Cao J, Arha M, Sudrik C, Schaffer DV, and Kane RS (2014) Bidirectional regulation of mRNA translation in mammalian cells by using PUF domains, Angew. Chem. Int. Ed. Engl 53, 4900–4904. [PubMed: 24677733]
27. Brechun KE, Arndt KM, and Woolley GA (2017) Strategies for the photo-control of endogenous protein activity, Curr. Opin. Struct. Biol 45, 53–58. [PubMed: 27907886]

28. Topisirovic I, Svitkin YV, Sonenberg N, and Shatkin AJ (2011) Cap and cap-binding proteins in the control of gene expression, Wiley Interdiscip. Rev. RNA 2, 277–298. [PubMed: 21957010]
29. Gruner S, Peter D, Weber R, Wohlbold L, Chung MY, Weichenrieder O, Valkov E, Igreja C, and Izaurralde E (2016) The structures of eIF4E-eIF4G complexes reveal an extended interface to regulate translation initiation, Mol. Cell 64, 467–479. [PubMed: 27773676]
30. Peter D, Igreja C, Weber R, Wohlbold L, Weiler C, Ebertsch L, Weichenrieder O, and Izaurralde E (2015) Molecular architecture of 4E-BP translational inhibitors bound to eIF4E, Mol. Cell 57, 1074–1087. [PubMed: 25702871]
31. Mizuno A, In Y, Fujita Y, Abiko F, Miyagawa H, Kitamura K, Tomoo K, and Ishida T (2008) Importance of C-terminal flexible region of 4E-binding protein in binding with eukaryotic initiation factor 4E, FEBS Lett. 582, 3439–3444. [PubMed: 18789325]
32. Bah A, Vernon RM, Siddiqui Z, Krzeminski M, Muhandiram R, Zhao C, Sonenberg N, Kay LE, and Forman-Kay JD (2015) Folding of an intrinsically disordered protein by phosphorylation as a regulatory switch, Nature 519, 106–109. [PubMed: 25533957]
33. Fletcher CM, McGuire AM, Gingras AC, Li H, Matsuo H, Sonenberg N, and Wagner G (1998) 4E binding proteins inhibit the translation factor eIF4E without folded structure, Biochemistry 37, 9–15. [PubMed: 9453748]
34. Herbert TP, Fahraeus R, Prescott A, Lane DP, and Proud CG (2000) Rapid induction of apoptosis mediated by peptides that bind initiation factor eIF4E, Curr. Biol 10, 793–796. [PubMed: 10898981]
35. Salaun P, Boulben S, Mulner-Lorillon O, Belle R, Sonenberg N, Morales J, and Cormier P (2005) Embryonic-stage-dependent changes in the level of eIF4E-binding proteins during early development of sea urchin embryos, J. Cell Sci 118, 1385–1394. [PubMed: 15769855]
36. Musa J, Orth MF, Dallmayer M, Baldauf M, Pardo C, Rotblat B, Kirchner T, Leprivier G, and Grunewald TG (2016) Eukaryotic initiation factor 4E-binding protein 1 (4E-BP1): a master regulator of mRNA translation involved in tumorigenesis, Oncogene 35, 4675–4688. [PubMed: 26829052]
37. Thoreen CC, Chantranupong L, Keys HR, Wang T, Gray NS, and Sabatini DM (2012) A unifying model for mTORC1-mediated regulation of mRNA translation, Nature 485, 109–113. [PubMed: 22552098]
38. Costello J, Castelli LM, Rowe W, Kershaw CJ, Talavera D, Mohammad-Qureshi SS, Sims PF, Grant CM, Pavitt GD, Hubbard SJ, and Ashe MP (2015) Global mRNA selection mechanisms for translation initiation, Genome Biol. 16, 10. [PubMed: 25650959]
39. Yanagiya A, Suyama E, Adachi H, Svitkin YV, Aza-Blanc P, Imataka H, Mikami S, Martineau Y, Ronai ZA, and Sonenberg N (2012) Translational homeostasis via the mRNA cap-binding protein, eIF4E, Mol. Cell 46, 847–858. [PubMed: 22578813]
40. Khaleghpour K, Pyronnet S, Gingras AC, and Sonenberg N (1999) Translational homeostasis: eukaryotic translation initiation factor 4E control of 4E-binding protein 1 and p70 S6 kinase activities, Mol. Cell. Biol 19, 4302–4310. [PubMed: 10330171]
41. Richter JD, and Sonenberg N (2005) Regulation of cap-dependent translation by eIF4E inhibitory proteins, Nature 433, 477–480. [PubMed: 15690031]
42. Volpon L, Culjkovic-Kraljacic B, Sohn HS, Blanchet-Cohen A, Osborne MJ, and Borden KLB (2017) A biochemical framework for eIF4E-dependent mRNA export and nuclear recycling of the export machinery, RNA 23, 927–937. [PubMed: 28325843]
43. Frydryskova K, Masek T, Borcin K, Mrvova S, Venturi V, and Pospisek M (2016) Distinct recruitment of human eIF4E isoforms to processing bodies and stress granules, BMC Mol. Biol 17, 21. [PubMed: 27578149]
44. Ferrero PV, Layana C, Paulucci E, Gutierrez P, Hernandez G, and Rivera-Pomar RV (2012) Cap binding-independent recruitment of eIF4E to cytoplasmic foci, Biochim. Biophys. Acta 1823, 1217–1224. [PubMed: 22507384]
45. Sukarieh R, Sonenberg N, and Pelletier J (2009) The eIF4E-binding proteins are modifiers of cytoplasmic eIF4E relocalization during the heat shock response, Am. J. Physiol. Cell. Physiol 296, C1207–1217. [PubMed: 19244480]

46. Joshi B, Cameron A, and Jagus R (2004) Characterization of mammalian eIF4E-family members, Eur. J. Biochem 271, 2189–2203. [PubMed: 15153109]
47. Joshi B, Robalino J, Schott EJ, and Jagus R (2002) Yeast “knockout-and-rescue” system for identification of eIF4E-family members possessing eIF4E-activity, Biotechniques 33, 392–393, 395–396, 398 passim. [PubMed: 12188192]
48. Rhoads RE, Dinkova TD, and Jagus R (2007) Approaches for analyzing the differential activities and functions of eIF4E family members, Methods Enzymol. 429, 261–297. [PubMed: 17913628]
49. Altmann M, Muller PP, Pelletier J, Sonenberg N, and Trachsel H (1989) A mammalian translation initiation factor can substitute for its yeast homologue in vivo, J. Biol. Chem 264, 12145–12147. [PubMed: 2663851]
50. Hughes JM, Ptushkina M, Karim MM, Koloteva N, von der Haar T, and McCarthy JE (1999) Translational repression by human 4E-BP1 in yeast specifically requires human eIF4E as target, J. Biol. Chem 274, 3261–3264. [PubMed: 9920863]
51. Ptushkina M, von der Haar T, Karim MM, Hughes JM, and McCarthy JE (1999) Repressor binding to a dorsal regulatory site traps human eIF4E in a high cap-affinity state, EMBO J. 18, 4068–4075. [PubMed: 10406811]
52. Zhou XX, Chung HK, Lam AJ, and Lin MZ (2012) Optical control of protein activity by fluorescent protein domains, Science 338, 810–814. [PubMed: 23139335]
53. Strickland D, Lin Y, Wagner E, Hope CM, Zayner J, Antoniou C, Sosnick TR, Weiss EL, and Glotzer M (2012) TULIPs: tunable, light-controlled interacting protein tags for cell biology, Nat. Methods 9, 379–384. [PubMed: 22388287]
54. Conrad KS, Bilwes AM, and Crane BR (2013) Light-induced subunit dissociation by a light-oxygen-voltage domain photoreceptor from Rhodobacter sphaeroides, Biochemistry 52, 378–391. [PubMed: 23252338]
55. Abiko F, Tomoo K, Mizuno A, Morino S, Imataka H, and Ishida T (2007) Binding preference of eIF4E for 4E-binding protein isoform and function of eIF4E N-terminal flexible region for interaction, studied by SPR analysis, Biochem. Biophys. Res. Commun 355, 667–672. [PubMed: 17316564]
56. Lee VH, Healy T, Fonseca BD, Hayashi A, and Proud CG (2008) Analysis of the regulatory motifs in eukaryotic initiation factor 4E-binding protein 1, FEBS J. 275, 2185–2199. [PubMed: 18384376]
57. Strickland D, Yao X, Gawlak G, Rosen MK, Gardner KH, and Sosnick TR (2010) Rationally improving LOV domain-based photoswitches, Nat. Methods 7, 623–626. [PubMed: 20562867]
58. Kumar A, Burns DC, Al-Abdul-Wahid MS, and Woolley GA (2013) A circularly permuted photoactive yellow protein as a scaffold for photoswitch design, Biochemistry 52, 3320–3331. [PubMed: 23570450]
59. Zayner JP, Antoniou C, and Sosnick TR (2012) The amino-terminal helix modulates light-activated conformational changes in AsLOV2, J. Mol. Biol 419, 61–74. [PubMed: 22406525]
60. Ali AM, Reis JM, Xia Y, Rashid AJ, Mercaldo V, Walters BJ, Brechun KE, Borisenko V, Josselyn SA, Karanicolas J, and Woolley GA (2015) Optogenetic inhibitor of the transcription factor CREB, Chem. Biol 22, 1531–1539. [PubMed: 26590638]
61. Kumar A, Ali AM, and Woolley GA (2015) Photo-control of DNA binding by an engrailed homeodomain-photoactive yellow protein hybrid, Photochem. Photobiol. Sci 14, 1729–1736. [PubMed: 26204102]
62. Halavaty AS, and Moffat K (2007) N- and C-terminal flanking regions modulate light-induced signal transduction in the LOV2 domain of the blue light sensor phototropin 1 from Avena sativa, Biochemistry 46, 14001–14009. [PubMed: 18001137]
63. Mader S, Lee H, Pause A, and Sonenberg N (1995) The translation initiation factor eIF-4E binds to a common motif shared by the translation factor eIF-4 gamma and the translational repressors 4E-binding proteins, Mol. Cell. Biol 15, 4990–4997. [PubMed: 7651417]
64. Robertson JB, Davis CR, and Johnson CH (2013) Visible light alters yeast metabolic rhythms by inhibiting respiration, Proc. Natl. Acad. Sci. U.S.A 110, 21130–21135. [PubMed: 24297928]
65. Zoltowski BD, Vaccaro B, and Crane BR (2009) Mechanism-based tuning of a LOV domain photoreceptor, Nat. Chem. Biol 5, 827–834. [PubMed: 19718042]

66. Ziegler T, and Moglich A (2015) Photoreceptor engineering, Front. Mol. Biosci 2, 30. [PubMed: 26137467]

67. Pudasaini A, El-Arab KK, and Zoltowski BD (2015) LOV-based optogenetic devices: light-driven modules to impart photoregulated control of cellular signaling, Front. Mol. Biosci 2, 18. [PubMed: 25988185]

68. Paku KS, Umenaga Y, Usui T, Fukuyo A, Mizuno A, In Y, Ishida T, and Tomoo K (2012) A conserved motif within the flexible C-terminus of the translational regulator 4E-BP is required for tight binding to the mRNA cap-binding protein eIF4E, Biochem J 441, 237–245. [PubMed: 21913890]

69. St Onge RP, Mani R, Oh J, Proctor M, Fung E, Davis RW, Nislow C, Roth FP, and Giaever G (2007) Systematic pathway analysis using high-resolution fitness profiling of combinatorial gene deletions, Nat. Genet 39, 199–206. [PubMed: 17206143]

70. Choi JH, San A, and Ostermeier M (2013) Non-allosteric enzyme switches possess larger effector-induced changes in thermodynamic stability than their non-switch analogs, Protein Sci. 22, 475–485. [PubMed: 23400970]

71. Culjkovic B, Topisirovic I, Skrabanek L, Ruiz-Gutierrez M, and Borden KL (2006) eIF4E is a central node of an RNA regulon that governs cellular proliferation, J. Cell Biol 175, 415–426. [PubMed: 17074885]

72. Dever TE, Kinzy TG, and Pavitt GD (2016) Mechanism and Regulation of Protein Synthesis in Saccharomyces cerevisiae, Genetics 203, 65–107. [PubMed: 27183566]

73. Pospisek M, and Valasek L (2013) Polysome profile analysis--yeast, Methods Enzymol. 530, 173–181. [PubMed: 24034321]

74. Hu W, and Coller J (2013) Polysome analysis for determining mRNA and ribosome association in Saccharomyces cerevisiae, Methods Enzymol 530, 193–206. [PubMed: 24034323]

75. Gilbert WV, Zhou K, Butler TK, and Doudna JA (2007) Cap-independent translation is required for starvation-induced differentiation in yeast, Science 317, 1224–1227. [PubMed: 17761883]

76. Zayner JP, and Sosnick TR (2014) Factors that control the chemistry of the LOV domain photocycle, PLoS One 9, e87074. [PubMed: 24475227]

77. Schwanhausser B, Busse D, Li N, Dittmar G, Schuchhardt J, Wolf J, Chen W, and Selbach M (2011) Global quantification of mammalian gene expression control, Nature 473, 337–342. [PubMed: 21593866]

78. Kapur M, Monaghan CE, and Ackerman SL (2017) Regulation of mRNA Translation in Neurons-A Matter of Life and Death, Neuron 96, 616–637. [PubMed: 29096076]

79. Cao J, Arha M, Sudrik C, Mukherjee A, Wu X, and Kane RS (2015) A universal strategy for regulating mRNA translation in prokaryotic and eukaryotic cells, Nucleic Acids Res. 43, 4353–4362. [PubMed: 25845589]

80. Abdou K, Shehata M, Choko K, Nishizono H, Matsuo M, Muramatsu SI, and Inokuchi K (2018) Synapse-specific representation of the identity of overlapping memory engrams, Science 360, 1227–1231. [PubMed: 29903972]

81. Buffington SA, Huang W, and Costa-Mattioli M (2014) Translational control in synaptic plasticity and cognitive dysfunction, Annu. Rev. Neurosci 37, 17–38. [PubMed: 25032491]

82. Hochrein L, Machens F, Messerschmidt K, and Mueller-Roeber B (2017) PhiReX: a programmable and red light-regulated protein expression switch for yeast, Nucleic Acids Res. 45, 9193–9205. [PubMed: 28911120]

83. McIsaac RS, Oakes BL, Wang X, Dummit KA, Botstein D, and Noyes MB (2013) Synthetic gene expression perturbation systems with rapid, tunable, single-gene specificity in yeast, Nucleic Acids Res. 41, e57. [PubMed: 23275543]

84. Hsiao K, Bozdagi O, and Benson DL (2014) Axonal cap-dependent translation regulates presynaptic p35, Dev. Neurobiol 74, 351–364. [PubMed: 24254883]

85. Wrenbeck EE, Faber MS, and Whitehead TA (2017) Deep sequencing methods for protein engineering and design, Curr. Opin. Struct. Biol 45, 36–44. [PubMed: 27886568]

86. Arndt N, Ross-Kaschitza D, Kojukhov A, Komar AA, and Altmann M (2018) Properties of the ternary complex formed by yeast eIF4E, p20 and mRNA, Sci. Rep 8, 6707. [PubMed: 29712996]

87. Rhoads RE (2009) eIF4E: new family members, new binding partners, new roles, J. Biol. Chem 284, 16711–16715. [PubMed: 19237539]

88. Tcherkezian J, Cargnello M, Romeo Y, Huttlin EL, Lavoie G, Gygi SP, and Roux PP (2014) Proteomic analysis of cap-dependent translation identifies LARP1 as a key regulator of 5'TOP mRNA translation, Genes Dev. 28, 357–371. [PubMed: 24532714]

89. Gosselin P, Martineau Y, Morales J, Czjzek M, Glippa V, Gauffeny I, Morin E, Le Corguille G, Pyronnet S, Cormier P, and Cosson B (2013) Tracking a refined eIF4E-binding motif reveals Angel1 as a new partner of eIF4E, Nucleic Acids Res. 41, 7783–7792. [PubMed: 23814182]

90. Kamenska A, Simpson C, and Standart N (2014) eIF4E-binding proteins: new factors, new locations, new roles, Biochem. Soc. Trans 42, 1238–1245. [PubMed: 25110031]

91. Hsieh AC, Costa M, Zollo O, Davis C, Feldman ME, Testa JR, Meyuhas O, Shokat KM, and Ruggero D (2010) Genetic dissection of the oncogenic mTOR pathway reveals druggable addiction to translational control via 4EBP-eIF4E, Cancer Cell 17, 249–261. [PubMed: 20227039]

92. Dowling RJ, Topisirovic I, Alain T, Bidinosti M, Fonseca BD, Petroulakis E, Wang X, Larsson O, Selvaraj A, Liu Y, Kozma SC, Thomas G, and Sonenberg N (2010) mTORC1-mediated cell proliferation, but not cell growth, controlled by the 4E-BPs, Science 328, 1172–1176. [PubMed: 20508131]

93. Zhang T, Lei J, Yang H, Xu K, Wang R, and Zhang Z (2011) An improved method for whole protein extraction from yeast Saccharomyces cerevisiae, Yeast 28, 795–798. [PubMed: 21972073]

94. Iizuka N, Najita L, Franzusoff A, and Sarnow P (1994) Cap-dependent and cap-independent translation by internal initiation of mRNAs in cell extracts prepared from Saccharomyces cerevisiae, Mol. Cell. Biol 14, 7322–7330. [PubMed: 7935446]

95. Masek T, Vopalensky V, Suchomelova P, and Pospisek M (2005) Denaturing RNA electrophoresis in TAE agarose gels, Anal. Biochem 336, 46–50. [PubMed: 15582557]

96. Volpon L, Osborne MJ, Topisirovic I, Siddiqui N, and Borden KL (2006) Cap-free structure of eIF4E suggests a basis for conformational regulation by its ligands, EMBO J. 25, 5138–5149. [PubMed: 17036047]

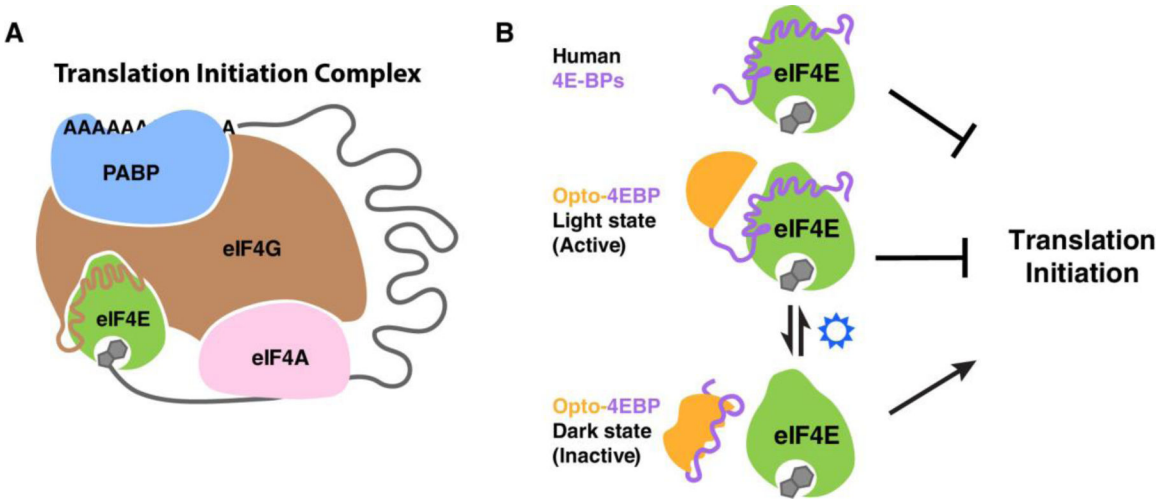

Figure 1. Optogenetic control of translation initiation

(A) Interactions in the eIF4F complex (eIF4G, eIF4E, eIF4A) and poly-A binding protein (PABP) during cap-dependent translation initiation. Binding and circularization of mRNA (gray) requires eIF4E and PABP. The 43S Preinitiation Complex (not shown) is then recruited to eIF4F and scans downstream of eIF4E for the start codon. **(B)** Native 4EBP binds eIF4E and inhibits translation initiation (top). Opto-4EBPs (represented by a photoswitchable domain in orange fused to a 4EBP segment in purple) have a sequestered 4EBP segment in the dark (bottom). Blue light irradiation causes a change in the photoswitchable domain and the 4EBP segment can adopt the conformation needed to bind eIF4E and inhibit translation initiation.

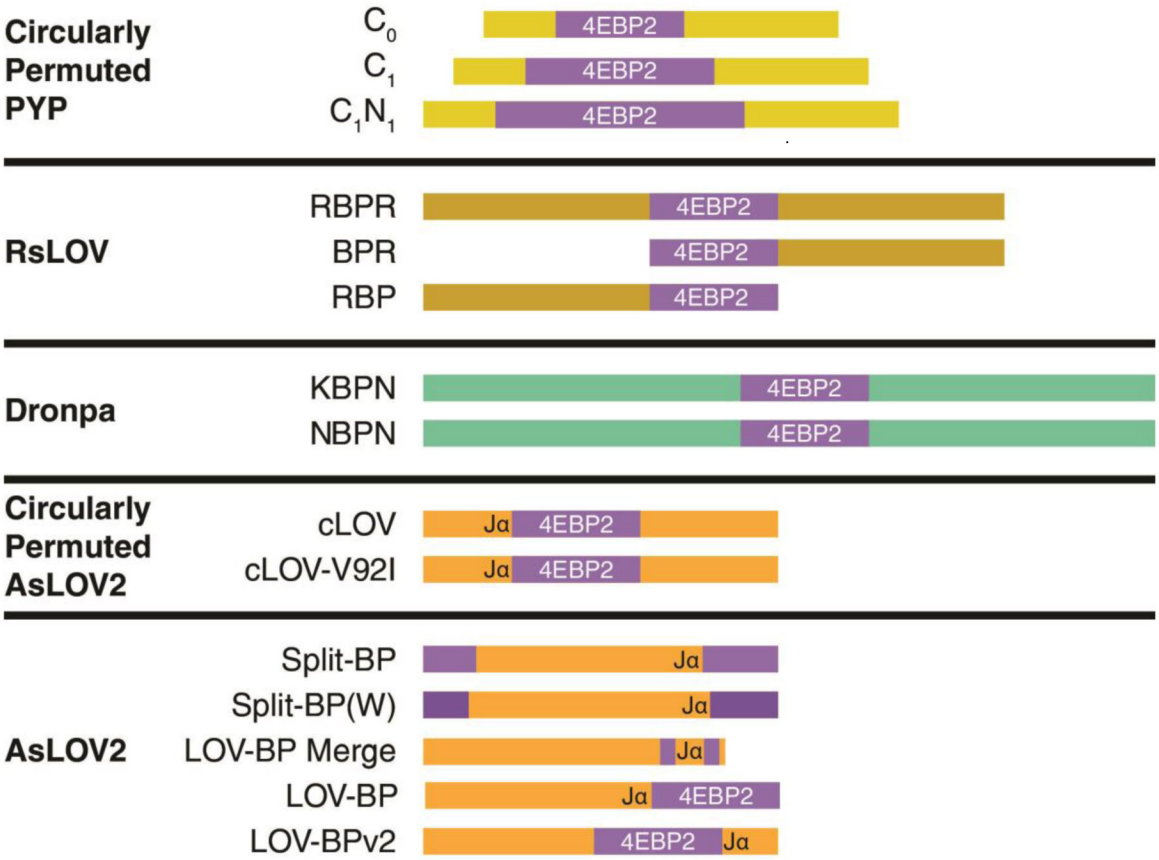

Figure 2.

Schematic of opto-4EBP2 designs screened in Jo56 yeast. Segments of 4EBP2 of varying lengths containing the primary and secondary eIF4E binding sites (shown in purple; a higher affinity 4EBP mimic[30] in dark purple) were fused in various configurations with different photoswitchable domains (cPYP, yellow; RsLOV, bronze; Dronpa, cyan; AsLOV2, cAsLOV2, orange).

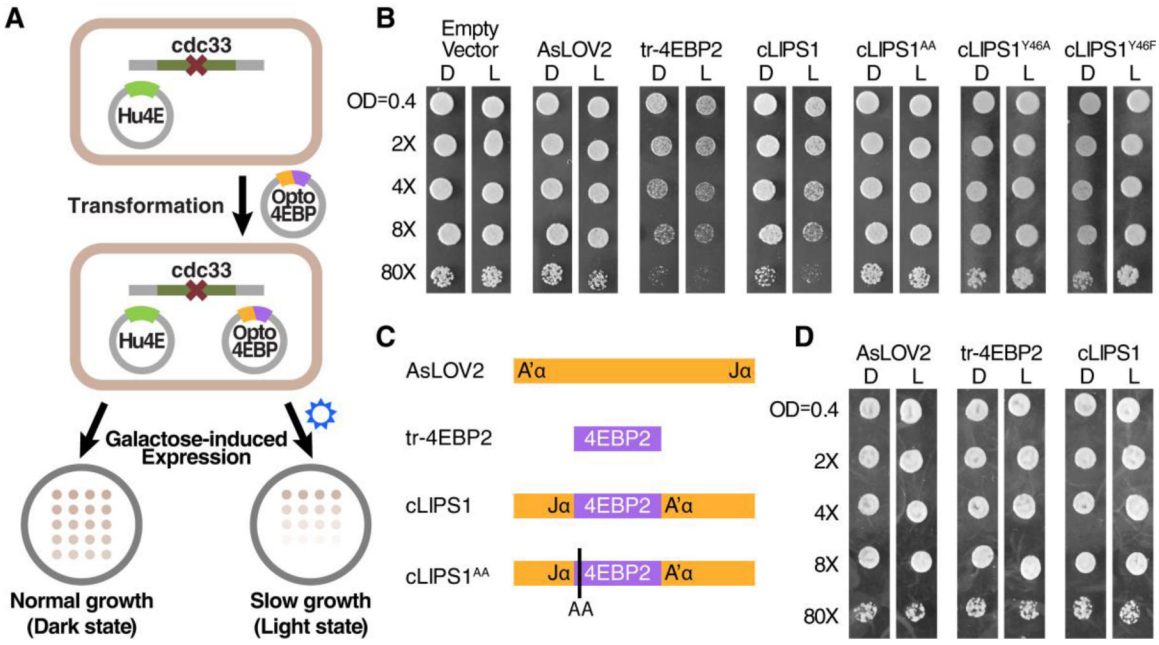

Figure 3. (A)

Schematic showing the yeast growth assay used to screen opto-4EBP constructs. Yeast (Jo56) with CDC33 deleted grow using constitutively expressed human eIF4E (green) expressed constitutively. This strain is transformed with opto-4EBPs (photoswitchable domain, orange; 4EBP2 segment, purple) and grown in glucose media for 2 days at 30°C. Transformed yeast are then plated on identical galactose plates to induce expression of opto-4EBPs. One plate is grown in the light and one plate is grown in the dark. Inhibition of growth in the light indicates light-activated inhibition of translation. **(B)** Yeast growth assay results for AsLOV2, tr-4EBP2, cLIPS1, and negative controls in drop test format. Cultures are spotted at the indicated ODs and growth is imaged after 3 days at 30°C under light (L) or dark (D) conditions. **(C)** Schematic of constructs (tr-4EBP2, cLIPS1 and controls) tested in yeast growth assay. The 4EBP2 (purple) insert is inserted between the Jα and A'α helices of AsLOV2. **(D)** Yeast growth assays using wild-type yeast (CB008) containing CDC33 (yeast eIF4E) and no human eIF4E. All constructs have no effect on growth indicating no interaction of 4EBPs with yeast eIF4E.

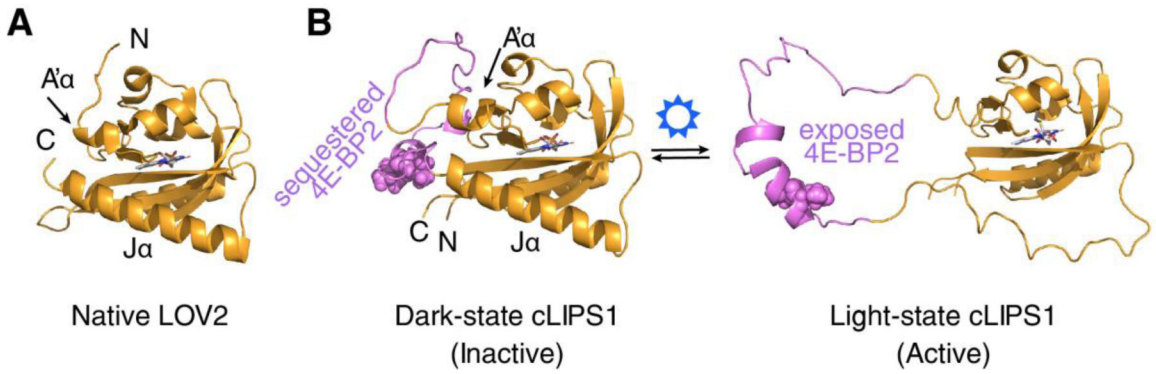

Figure 4. (A)
Crystal structure of dark-adapted AsLOV2 (PDB: 2V0U) **(B)** Hypothetical model of photoswitching of cLIPS1. The model was created by inserting the truncated 4EBP2 sequence (purple) between the N-terminal and C-terminal ends of AsLOV2, and creating new N- and C-termini (indicated) in AsLOV2. In the dark, cLIPS1 is proposed to fold so that primary and secondary eIF4E binding sites in 4EBP are sequestered. In the light, unfolding of the AsLOV2 Jα and A'α helices releases conformational constraints on 4EBP2 enabling it to adopt a conformation capable of binding to eIF4E. Structures of 4EBP2 segments and light state conformations of Jα and A'α helices are hypothetical.

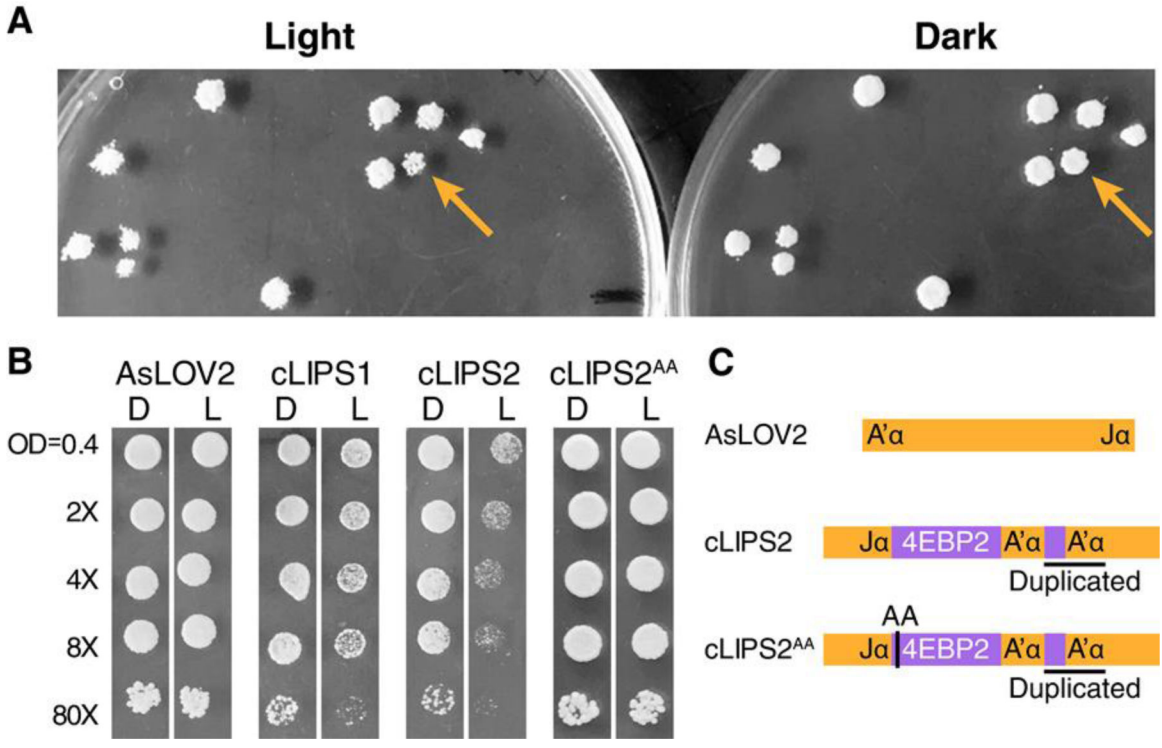

Figure 5. (A)

Image showing replica plates of yeast colonies grown from the primer-based library. One colony (cLIPS2, indicated by an arrow) showed distinctly less growth when grown in the light vs. in the dark. (B) Drop test assay of cLIPS2 compared to AsLOV2 and cLIPS1 (conditions as in Fig. 3B) (C) Schematic of cLIPS2 and cLIPS2^{AA} compared to AsLOV2. The duplicated section is composed of a portion of 4EBP2 (purple) that encompasses the secondary binding site and the A'α helix of AsLOV (orange, indicated).

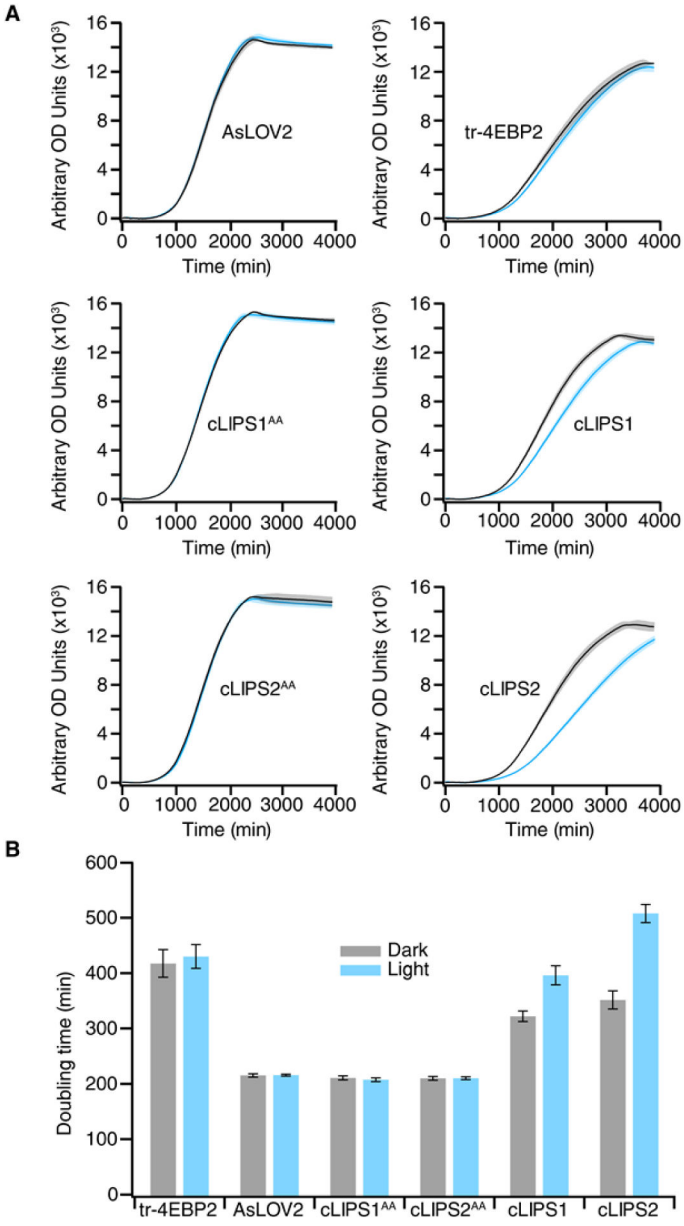

Figure 6. (A)

Growth curves of Jo56 yeast expressing AsLOV2, tr-4EBP2, cLIPS1, cLIPS1^{AA}, cLIPS2, or cLIPS2^{AA}. Yeast were grown in the dark (black lines), and in the light (blue lines) in an automated shaker and plate reader. Shaded area (dark state, grey; light state, light blue) shows the error between wells in 3 different experiments. Each light or dark experiment was performed with 8–16 wells per construct. **(B)** Calculated doubling times based on the measured growth curves. Error bars represent standard deviation between three separate experiments.

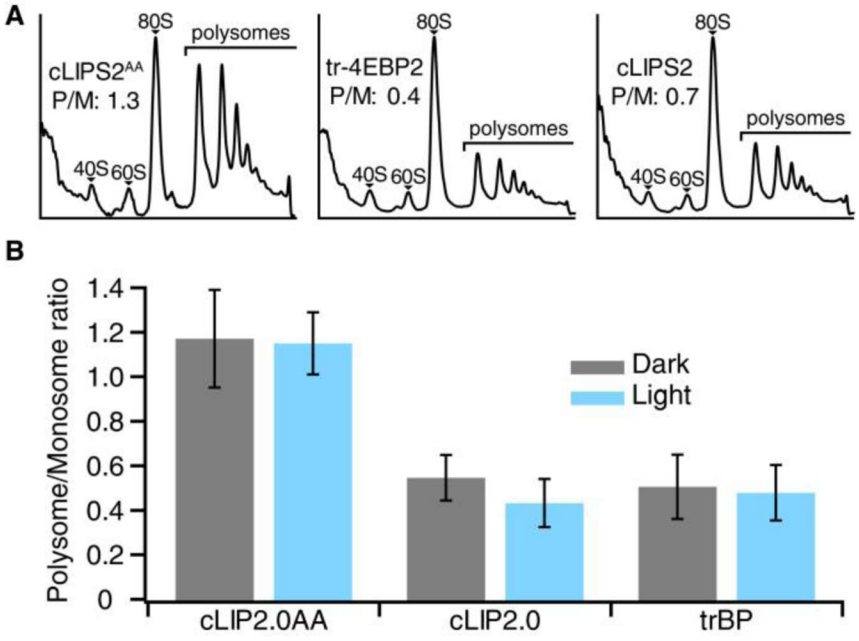

Figure 7. (A)

Representative polysome profiles for Jo56 expressing cLIPS2^{AA}, tr-4EBP2, or cLIPS2, grown in the dark. Polysome/monosome (P/M) ratios are indicated for these individual profiles. **(B)** Bar plot showing the average P/M ratio for three polysome profiling experiments. In each replicate, Jo56 yeast expressing cLIPS2^{AA}, tr-4EBP2, and cLIPS2 were either grown in the light (30 s on and off, 0.05 mW/cm^2 blue light) or in the dark until early log phase. Error bars represent the standard deviation between three separate experiments.

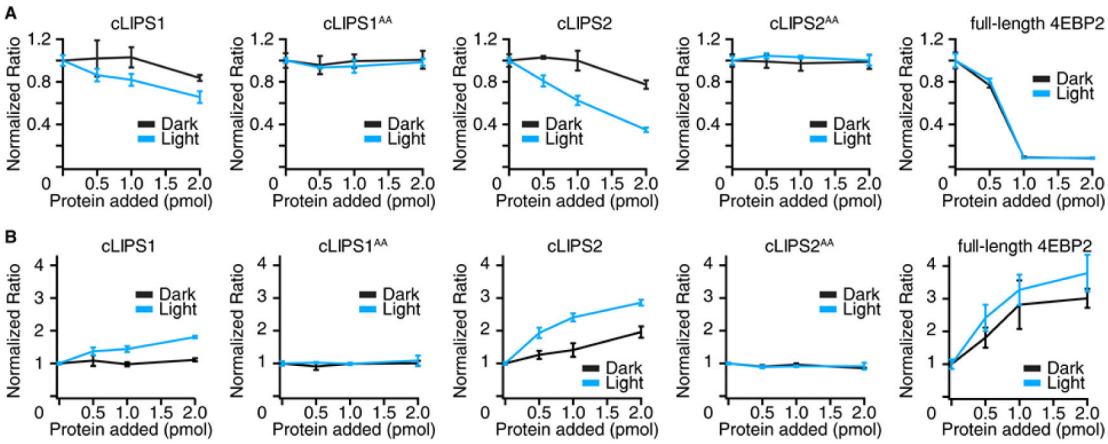

Figure 8. (A)

In vitro translation assays using Jo56 lysates with capped (‘eIF4E-sensitive’) mRNA expressing Renilla luciferase. Purified cLIPS constructs or full-length 4EBP2 were added in increasing amounts under either dark or light conditions. Whereas full-length 4EBP2 causes inhibition regardless of light conditions, cLIPS1 and cLIPS2 cause light-dependent inhibition of cap-dependent translation. The AA controls show no inhibition of translation. **(B)** In vitro translation assays using Jo56 lysates with PAB1 IRES mRNA coding for Renilla luciferase. In this case full-length 4EBP2 causes enhanced translation, cLIPS1 and cLIPS2 cause light-dependent enhancement of translation. The AA controls show no effect on translation.

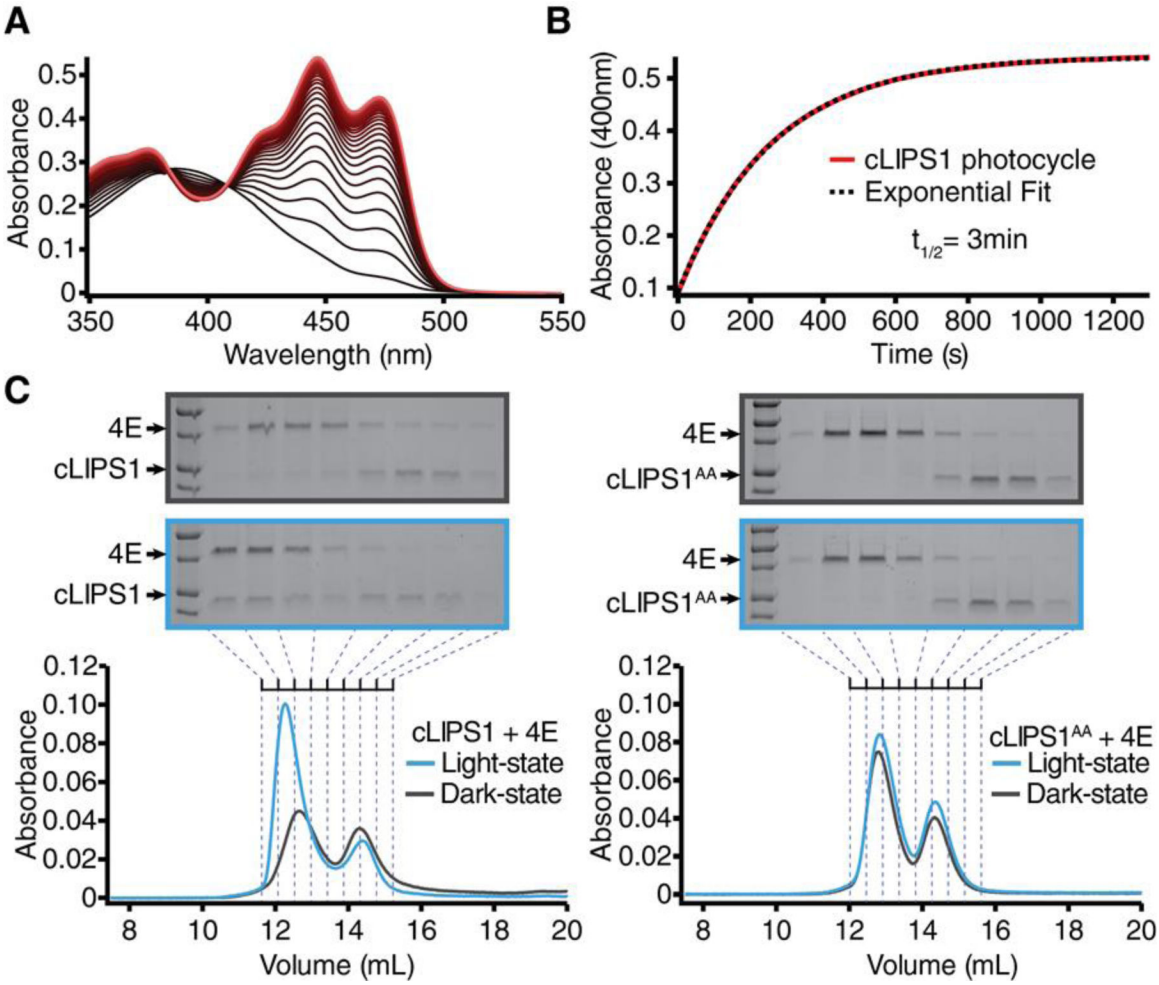

Figure 9. (A)

UV-Vis spectra showing the cLIPS1 photocycle after 1 min irradiation with 450 nm light. (50 mM sodium phosphate (pH 6.5), 100 mM NaCl, and 1 mM DTT, 25°C). **(B)** Time course of cLIPS1 thermal recovery calculated from the set of UV-Vis spectra. Absorbance at 450 nm vs time was fitted to an exponential curve and the half-life calculated was ~3 min. **(C)** SEC chromatographs of either cLIPS1 (left chromatograph, 10 μM) or cLIPS1^{AA} (right chromatograph, 10 μM) mixed with eIF4E (10 μM) in the dark (black lines) or under constant irradiation of 450 nm light (blue lines). Fractions of the chromatograph (indicated) were collected and analyzed using SDS-PAGE. With eIF4E and cLIPS1, co-elution occurs at earlier fractions under 450 nm light. With eIF4E and cLIPS1^{AA}, no co-elution is seen in either light or dark conditions.